HHS Public Access

Author manuscript

Nature. Author manuscript; available in PMC 2020 September 18.

Published in final edited form as:

Nature. 2020 April ; 580(7801): 130–135. doi:10.1038/s41586-020-2121-3.

Metabolites released from apoptotic cells act as novel tissue messengers

Christopher B. Medina[1,2], **Parul Mehrotra**[7,*], **Sanja Arandjelovic**[1,2,*], **Justin S.A. Perry**[1,2,*], **Yizhan Guo**[3], **Sho Morioka**[1,2], **Brady Barron**[1,4], **Scott F. Walk**[1,2], **Bart Ghesquière**[6], **Alexander S. Krupnick**[3,5], **Ulrike Lorenz**[2,5], **Kodi S. Ravichandran**[1,2,5,7]

[1]Center for Cell Clearance, University of Virginia, Charlottesville, VA

[2]Department of Microbiology, Immunology, and Cancer Biology, University of Virginia, Charlottesville, VA

[3]Department of Surgery, University of Virginia, Charlottesville, VA

[4]Pharmacology, University of Virginia, Charlottesville, VA

[5]Carter Immunology Center, University of Virginia, Charlottesville, VA

[6]Department of Oncology and VIB, KULeuven, Belgium

[7]VIB/UGent Inflammation Research Centre, Biomedical Molecular Biology, Ghent University, Belgium

Abstract

Caspase-dependent apoptosis accounts for ~90% of homeostatic cell turnover in the body[1], and regulates inflammation, cell proliferation, and tissue regeneration[2–4]. How apoptotic cells mediate such diverse effects is not fully understood. Here, we profiled the apoptotic 'metabolite secretome' and addressed their effects on the tissue neighborhood. Apoptotic lymphocytes and macrophages release specific metabolites, while retaining their membrane integrity. A subset of these metabolites is also shared across different primary cells and cell lines after apoptosis induction by different stimuli. Mechanistically, apoptotic metabolite secretome was not due to passive emptying of contents, rather orchestrated. First, caspase-mediated opening of the plasma membrane Pannexin 1 channels facilitated release of a select subset of the metabolite secretome. Second,

Correspondence and requests for materials should be addressed to K.S.R. (Ravi@virginia.edu).

*contributed equally to this work

Author Contributions

C.BM. and K.S.R designed the experiments. C.B.M. performed majority of the experiments. P.M.M. performed the macrophage apoptosis and polyamine tracing experiments. S.A. and C.B.M performed the arthritis experiments. J.S.A.P. assisted with the bioinformatic analyses. Y.G. and A.S.K. assisted with the lung transplant experiments. S.M., B.B., and S.W. provided experimental expertise on few specific experiments. B.G. assisted with the polyamine mass-spectrometry and U.L. provided mice and conceptual advice. C.B.M. and K.S.R wrote the manuscript with input from coauthors.

Competing Interests. The authors declare no competing interests.

Data Availability. RNAseq data have been submitted to the Gene Expression Omnibus under accession number GSE131906. Other data that support the findings of this study are available from the corresponding author upon request.

Code Availability. Codes are available from the corresponding author upon request.

certain metabolic pathways continue to remain active during apoptosis, with release of select metabolites from a given pathway. Functionally, the apoptotic metabolite secretome induced specific gene programs in healthy neighboring cells, including suppression of inflammation, cell proliferation, and wound healing. Further, a cocktail of select apoptotic metabolites reduced disease severity in mouse models of inflammatory arthritis and lung graft rejection. These data advance the concept that apoptotic cells are not 'inert corpses' waiting for removal, rather release metabolites as 'good-bye' signals that actively modulate tissue outcomes.

Apoptosis occurs during development[3], homeostatic tissue turnover, and pathological settings[1]. Besides the known responses of phagocytes that engulf apoptotic cells[4], the apoptotic process itself (independent of phagocytosis), can modulate physiological events, such as embryogenesis and tissue regeneration[5], with pathologies arising when apoptosis is inhibited[6]. However, the mechanisms by which apoptotic cells themselves mediate these functions are incompletely understood. As apoptotic cells remain intact for a period of time, they could release soluble metabolites that diffuse within a tissue to influence neighboring cells. Although a few soluble factors from apoptotic cells are reported as 'find-me' signals to attract phagocytes[7], the full apoptotic secretome is not yet defined.

To profile the metabolite secretome of apoptotic cells, we used human Jurkat T cells, primary murine thymocytes, or primary bone-marrow derived macrophages (BMDM), all of which can undergo inducible, caspase-dependent apoptosis (UV treatment, anti-Fas antibody crosslinking, or anthrax lethal toxin-induced apoptosis)[8,9](Fig. 1a). As untargeted metabolomics require large numbers of cells, we optimized the parameters using Jurkat cells (e.g. cell density, culture volume, duration after apoptosis), such that ~80% of the cells were apoptotic, while maintaining cell membrane integrity (Annexin V^+7AAD^-) (Extended Data 1a, b). Supernatants and cell pellets from apoptotic and live cell controls were subjected to untargeted metabolomic profiling against a library of >3000 biochemical features/ compounds. Supernatants of apoptotic Jurkat cells (UV) showed an enrichment of 123 metabolites (Fig. 1b, Extended Data 1c, d, Supplementary Table 1), and 85 of these 123 were reciprocally reduced in the apoptotic cell pellets (Extended Data 2a–f, Supplementary Table 2).

In untargeted metabolomics of supernatants from macrophages undergoing apoptosis (via anthrax lethal toxin[9]), we detected fewer metabolites (20, versus 123 in Jurkat cells), perhaps due to differences in cell types, modality of death and/or quantities released (i.e. detection limits). Strikingly, 16 of the 20 metabolites (80%) were shared with apoptotic Jurkat cells (Fig. 1b).

For further validation and quantitation, we performed 'targeted metabolomics' analyzing 116 specific metabolites (see methods) on supernatants from Jurkat cells and primary murine thymocytes after Fas-crosslinking ('extrinsic' cue for apoptosis) (Supplementary Table 3). This targeted panel included 43 of the metabolites released from apoptotic Jurkat cells (identified above), and included a 5kDa filtering step (to exclude proteins, and extracellular vesicles). This targeted analysis showed an enrichment of many metabolites seen with UV-induced apoptosis (Fig. 1b). Further, metabolites released from apoptotic primary thymocytes overlapped with apoptotic Jurkat cells (Fig. 1b). Comparing metabolites

enriched/released in the apoptotic supernatant of Jurkat cells, thymocytes, and macrophages (after Fas, UV, or toxin-mediated apoptosis) identified five 'conserved' metabolites: AMP, GMP, creatine, spermidine, and glycerol 3-phosphate (Fig. 1b, Extended Data 3a). ATP represents the 6th shared metabolite (via luciferase assay, Extended Data 3b), although ATP was not profiled in the metabolomics.

To test other cell types and additional apoptotic modalities, we analyzed the release of four 'conserved metabolites' via analytical kits. Jurkat cells, A549 lung epithelial cells, and HCT116 colonic epithelial cells were induced to undergo death via different apoptotic cues, such as UV, BH3-mimetic ABT-737 (which directly induces mitochondrial outer membrane permeabilization), and/or TRAIL (extrinsic mode of apoptosis) (Fig. 1c–e). We could readily detect apoptosis-dependent release of the tested metabolites, and attenuation by pan-caspase inhibitor zVAD (Fig. 1c–e, Extended data 3c). The metabolites detected were not due to simple emptying of cellular contents during apoptosis, as many metabolites at high intracellular concentrations were not released (Fig. 1f). These data reveal apoptotic cells as a novel 'natural source' of many metabolites with biological functions.

During the above analyses, we noted that despite the many cellular metabolites detected in the pellet, only a subset is released; further, even within a known metabolic pathway, only some but not others were released. Such selectivity could arise from either specific channels opening during apoptosis to permeate certain metabolites, and/or continued metabolic activity within the dying cell influencing the secretome. To test specific channels, we focused on pannexin 1 (Panx1) channels that are activated during apoptosis by caspase-mediated cleavage[10] and can conduct ions and small molecules up to 1kDa in size across the plasma membrane. In a Panx1-dependent manner[10], apoptotic cells (not live cells) take up TO-PRO-3 (671 Daltons) dye, while 7AAD (1.27 kDa) is excluded (Extended Data 4a, b). We tested the relevance of Panx1 by genetic and pharmacological approaches. Genetically, we used Jurkat cells expressing a dominant negative Panx1 with a caspase cleavage site mutation[10] (Panx1-DN) or primary thymocytes from Panx1-deficient mice (*Panx1*$^{-/-}$)[11]. We also used two pharmacological inhibitors, trovafloxacin (Trovan) and spironolactone (Spiro), which we had previously identified in unbiased screens[11,12]. Disrupting Panx1 activity *per se* did not affect apoptosis (Extended Data 5a–e). Untargeted metabolomics of the supernatants from apoptotic Jurkat cells (UV-induced) with and without Panx1 inhibition revealed that Panx1 contributed to release ~20% of the apoptotic metabolites (25 out of 123) (Fig. 2a, Extended Data 6a). The Panx1-dependent metabolites included nucleotides, nucleotide-sugars, and metabolites linked to energy metabolism and amino acid metabolism; interestingly, most have not been previously reported to permeate through Panx1. A similar Panx1-dependent metabolite signature was shared between Jurkat cells and thymocytes; further, as not all apoptotic metabolites released were Panx1-dependent, other mechanisms must also exist (Extended Data 6b–e). We noted eight shared Panx1-dependent apoptotic metabolites between Jurkat cells and primary thymocytes (Fig. 2b and Extended Data 7).

To test whether the apoptotic secretome might also be influenced by the metabolic activity within the dying cell, we chose the polyamine pathway for several reasons. First, the polyamine spermidine was released in significant quantities from apoptotic Jurkat cells, macrophages, thymocytes, and epithelial cells after different modes of apoptosis induction

(Fig. 2c). Second, among the two metabolites immediately upstream of spermidine, putrescine was not released, while ornithine was present comparably in live and apoptotic cell supernatants (Fig. 2d). Third, while exogenous spermidine supplementation can reduce inflammation and improve longevity[13], spermidine release from apoptotic cells provides the first *natural/physiological* extracellular source of this polyamine.

The upstream steps of spermidine generation involve arginine→ ornithine→ putrescine→ spermidine, with each conversion regulated by specific enzymes. A recent report[14] showed that while the majority of mRNA gets degraded in apoptotic HCT-116 cells, a small fraction is 'retained'. In our re-analysis of this mRNA dataset, the polyamine pathway enzyme transcripts were not degraded during apoptosis, including spermidine synthase (SRM) that converts putrescine to spermidine (Extended data 8a)[14]. We confirmed that in apoptotic Jurkat cells, the mRNA for spermidine synthase was retained (Extended data 8b). To address this more directly by metabolic flux labeling, we added ^{13}C-Arginine medium to Jurkat cells immediately prior to apoptosis induction, and traced the label incorporation into putrescine and spermidine for the next few hours (Fig. 2e). Apoptotic cells displayed increased ^{13}C label incorporation into the polyamine pathway in the first hour, compared to live cells. After normalizing for total label incorporation and focusing on the carbons within the polyamine pathway (see methods), apoptotic cells showed 40% and 25% greater ^{13}C label/min incorporation into putrescine and spermidine, respectively, during the first hour (Fig. 2f). Although this dips during the 2nd hour, it was still comparable to live cells. Further, ^{13}C-labelled spermidine was detectable in the supernatants of apoptotic cells, and this was partially reduced by inhibition of caspases (Extended Data 8c). Interestingly, despite its active generation (revealed by ^{13}C labeling), putrescine was not detectable in apoptotic cell supernatants from Jurkat cells (or in the macrophage or thymocytes data set) (Fig. 2d). Thus, apoptotic cells orchestrate the generation and release of select metabolites at least at two levels – caspase-dependent opening of specific channels (Panx1) and continued metabolic activity of certain pathways.

To test whether released apoptotic cell-derived metabolites signal to alter gene expression programs in healthy nearby cells such as phagocytes, we added supernatants from live or apoptotic Jurkat cells (same conditions as untargeted metabolomics) to LR73 cells, a model phagocyte useful in revealing mechanisms/responses after efferocytosis[15–17] (Fig. 3a). RNAseq analysis of LR73 cells (after 4hr) indicated distinct transcriptional changes (Fig. 3b and Extended Data 9a). Pathway analysis, by hand-curating each of the hits individually, together with commonly used analysis software, revealed that the apoptotic secretome altered gene programs linked to cytoskeletal rearrangements, inflammation, wound healing/ tissue repair, anti-apoptotic functions, metabolism, and regulation of cell size within the phagocyte (Fig. 3b), providing a molecular and metabolic basis for how apoptosis may influence essential tissue processes.

By comparing gene programs induced in live cells by supernatants from apoptotic cells versus conditions with genetic inhibition of Panx1, we identified 110 genes as differentially regulated on phagocytes by Panx1-dependent apoptotic metabolites (82 up and 28 down) (Fig. 3c); these include genes involved in anti-inflammatory processes, anti-apoptotic pathways, metabolism, and actin rearrangement (Fig. 3c). Secondary validation via qPCR

indicates that Panx1-dependent metabolites can alter genes linked to anti-inflammatory roles in phagocytes (*Nr4a1, Pbx1*)[18,19], wound healing (*Areg, Ptgs2*)[20,21], and metabolism (*Slc14a1, Sgk1, Uap1*)[15,22] (Fig. 3d and Extended Data 9b). Furthermore, filtration of supernatants through 3kDa filters, prior to addition to phagocytes showed similar gene transcriptional changes (Extended Data 9c), ruling out larger proteins or vesicles from dying cells. Thus, metabolites released from apoptotic cells, a subset of which are released in a Panx1-dependent manner, can alter selective gene programs in the surrounding cells that sense these metabolic signals.

To test whether apoptotic Panx1-dependent metabolites can induce gene expression changes in tissue phagocytes *in vivo*, we used *Panx1*$^{fl/fl}$*Cd4*-Cre mice[11], where *Panx1* is targeted for deletion only within the thymocytes (Extended Data 10a left). After confirming that *Panx1* was not deleted in the macrophages and dendritic cells (Extended Data 10a right), and that comparable dexamethasone-induced thymocyte apoptosis occurs in control and *Panx1*$^{fl/fl}$*Cd4*-Cre mice (Extended Data 10b, c), we isolated CD11b^{+} macrophages and CD11c^{+} dendritic cells from the thymus and analyzed gene expression changes (Extended Data 10d, e). In wild-type mice, dexamethasone-induced apoptosis of thymocytes resulted in increased expression of *Uap1, Ugdh,* and *Pbx1* in surrounding live myeloid cells (linked to anti-inflammatory macrophage skewing/glycosylation and IL-10 transcription)[19,23] (Fig. 4a). This response was attenuated in mice lacking Panx1 channels in the dying thymocytes (Fig. 4a). Thus, apoptotic Panx1-dependent metabolites can induce gene expression changes in the surrounding tissue myeloid cells *in vivo*.

When tested individually, many of the metabolites failed to strongly induce anti-inflammatory and tissue-repair genes from the RNAseq (not shown). As these metabolites are concurrently released from apoptotic cells (Fig. 1), we tested mixtures of 6 of the 8 Panx1-dependent metabolites (Fig. 2b) in two combinations: i) spermidine, fructose-1,6-bis-phosphate, dihydroxyacetone phosphate, UDP-glucose, guanosine monophosphate, and inosine monophosphate; and ii) spermidine, guanosine monophosphate, and inosine monophosphate (Fig. 4b). All six have been previously administered *in vivo* in mice (or rats) without toxicity (Supplementary Table 4). We excluded AMP and glycerol-3-phosphate, as AMP can be converted to adenosine, a known anti-inflammatory metabolite, and it was difficult to determine the optimal *in vivo* dose for glycerol-3-phosphate. The metabolite mixtures were quite potent in inducing gene expression *in vitro*, including genes linked to anti-inflammatory macrophage skewing/glycosylation (*Uap1, Ugdh)*[23], IL-10 transcription and inflammation resolution (*Pbx1* [19], *Ptgs2* [24]), and metabolic processes (*Slc14a1, Sgk1),* some of which have also been shown to be involved in phagocytosis[15] (Fig. 4c). For simplicity, we have denoted the *me*tabolite *mix*tures as *MeMix*^{6} and *MeMix*^{3} (Fig. 4b).

Given the anti-inflammatory gene signature induced by the metabolites, we next tested *MeMix*^{6} and/or *MeMix*^{3} in attenuating inflammation *in vivo* in two contexts: a model of inflammatory arthritis, and a model of lung transplant rejection. For arthritis injection, a single injection of the arthritic serum from K/BxN mice into C57BL/6J mice results in inflammation of the joints with progressive arthritic symptoms, followed by disease resolution[25]. Of relevance to our question, this arthritis model is dependent on myeloid cells[25], with apoptosis known to occur during disease. We first asked whether the ‘full’

apoptotic secretome could alleviate inflammation in this arthritis model, and this was the case (Extended Data 10f). Administration of *MeMix*[6] or *MeMix*[3] after arthritis induction when the disease symptoms are noticeable resulted in significant attenuation of paw swelling and other arthritic parameters, compared to vehicle controls (Fig. 4d). Since fructose 1,6-bisphosphate (FBP) alone can have ameliorative roles in arthritis[26], we tested *MeMix*[3], which does not contain FBP. *MeMix*[3] not only alleviated paw swelling and external clinical arthritis parameters, but also significantly protected the joints from inflammation, bone erosion, and cartilage erosion (Fig. 4e, f).

We also tested *MeMix*[3] in a lung transplant rejection model, where local innate and adaptive immune responses orchestrated by graft-resident antigen presenting myeloid cells, dictate graft acceptance or rejection. We transplanted C57BL/10 left lung allografts to a minor antigen mismatched C57BL/6 recipient (Fig. 4g)[27], treating the graft recipients with *MeMix*[3] or saline vehicle control on post-operative days 1 and 3. On day 7 post-engraftment, saline-treated control mice showed severe acute rejection of allografts[28]. Remarkably, *MeMix*[3] treated mice had only minimal inflammation in the transplanted lungs (Fig. 4h), suggestive of amelioration of lung rejection. Complementary flow cytometric analysis of the lung showed reduced CD4 and CD8 cells in the transplanted lung of mice treated with *Memix* [3]. Thus, a subset of apoptotic metabolites can be harnessed for beneficial effects in two different inflammatory settings *in vivo*.

Collectively, the data presented here advance several concepts. First, we identify specific metabolites that are released from apoptotic cells (different cell types and modes of apoptosis induction); the specificity could arise from metabolic changes in the apoptotic cells (e.g. sustained spermidine production), and/or the opening of specific channels (e.g. Panx1). Second, apoptotic cells are not inert awaiting removal; rather, via metabolites as ‘good-bye’ signals modulate multiple gene programs in the neighboring cells within a tissue. Third, the ability of a cocktail of apoptotic metabolites to attenuate arthritic symptoms and lung transplantation rejection provides a proof-of-concept that it is possible to harness the beneficial therapeutic properties of apoptosis in specific inflammatory conditions.

Methods

Reagents

Trovafloxacin, spironolactone, dexamethasone, spermidine, fructose 1,6-bisphosphate, dihydroxyacetone phosphate, inosine 5’-monophosphate, and guanosine 5’-monophosphate were obtained from Sigma. UDP-glucose was obtained from Abcam and Annexin V-Pacific Blue was from BioLegend. 7AAD, TO-PRO-3, anti-CD11b-PE (clone M1/70), anti-CD11c-PE (clone N418), and anti-CD16/CD32 (clone 93) were obtained from Invitrogen. Antibodies specific for mouse CD95 were obtained from BD. Human anti-Fas (clone CH11) was obtained from Millipore. Other reagents were obtained as follows: ABT-737 (abcam), TRAIL (Sigma), and zVAD-FMK (Enzo).

Mice

C57BL/10 and C57BL/6J wild-type mice were acquired from Jackson Laboratories. *Panx1*$^{fl/fl}$ and *Panx1*$^{-/-}$ mice have been described previously[11]. To generate mice with deletion of *Panx1* in thymocytes, *Panx1*$^{fl/fl}$ mice were crossed to *Cd4*-Cre mice (Taconic). KRN TCR transgenic mice were a gift from Dr. Diane Mathis at the Harvard Medical School, and were bred to NOD mice (Jackson Laboratories) to obtain the K/BxN mice, which develop progressive spontaneous arthritis[29]. K/BxN serum was collected from 9-week old K/BxN mice by cardiac puncture. Animal procedures were approved and performed according to the Institutional Animal Care and Use Committee (IACUC) at the University of Virginia.

Apoptosis induction

Wild type Jurkat E6.1 (ATCC) or dominant negative Pannexin1-expressing (Panx1-DN)[10] cells were resuspended in RPMI-1640 containing 1% BSA, 1% PSQ, and 10mM HEPES and treated with 250 ng ml^{-1} anti-Fas (clone CH11), 10μM ABT-737, or exposed to 150mJ cm^{-2} ultraviolet C irradiation for 1-2 min (Stratalinker). Jurkat cells were incubated for 4 hours after apoptosis induction. For apoptosis induction in the presence of Panx1 inhibitors, Jurkat cells were treated with spironolactone (50μM) or trovafloxacin (25μM) in RPMI containing 1% BSA and 1% PSQ.

Primary thymocytes isolated from 4 to 6-week old wild-type or *Panx1*$^{-/-}$ mice were treated with 5 μg ml^{-1} anti-Fas (clone Jo2), that was subsequently crosslinked with 2 μg ml^{-1} protein G. Primary thymocytes were incubated for 1.5 hours after apoptosis induction.

B6$^{Nlrp1b+}$*C1*$^{-/-}$*C11*$^{-/-}$ were a gift from Dr. Mohamed Lamkanfi's lab (VIB/UGent, Belgium). BMDMs were generated by culturing mouse bone marrow cells in RPMI media conditioned with 10% dialyzed serum and 1% Pen-strep. The medium was supplemented with 20ng/ml of purified mouse M-CSF. Cells were incubated in a humidified atmosphere containing 5% CO_2 for 6 days. WT B6 or *B6*$^{Nlrp1b+}$*C1*$^{-/-}$*C11*$^{-/-}$ BMDMs were seeded in 6-well plates and, the next day, either left untreated or stimulated with 500 ng/mL with anthrax PA (500 ng/mL, Quadratech) and LF (250 ng/mL, Quadratech). Supernatants from either untreated or treated BMDMs was collected. Cellular debris was removed via centrifugation step and the clarified supernatant was used for metabolic profiling.

A549 cells were treated with 10μM ABT-737 or exposed 600mJ cm^{-2} and incubated for twenty-four hours. HCT-116 cells were treated with 10μM ABT-737 or 100ng ml^{-1} TRAIL and incubated for 24 hours. All cells were pre-treated for 10 min with 50uM zVAD prior to apoptosis induction in indicated experiments. All cells were incubated at 37 °C with 5% CO_2 for indicated times.

Metabolite detection

Spermidine detection was measured using a colorimetric kit (Cloud-Clone Corp.) via manufacturers' protocol. Briefly, supernatants taken from cells under specified conditions were centrifuged at 1000 x g for twenty minutes. All reagents were brought to room temperature prior to use. 50μl of sample were added to each well followed by equal volume

of Detection Reagent A and the plate was mixed. Samples were incubated, covered, for one hour at 37 °C. Wells were washed with 1x Wash solution three times before addition of Detection Reagent B, after which samples were incubated for another thirty minutes at 37 °C. Samples were washed again five times. 90μl of substrate solution was added to each well and incubated for 10 minutes at 37 °C after which 50μl of stop solution was added, the plate was mixed and immediately measure at 450nm on a plate reader (Flex station 3). Analysis was performed by back calculation to the standard curve, background subtraction and normalization to live cell controls.

ATP was measure using a luciferase-based kit (Promega) via manufactures' protocol. All reagents were equilibrated to room temperature before use. Briefly, supernatants taken from cells under specified conditions, were immediately moved to ice, and centrifuged at 500 x g for 5 minutes. Samples were placed back on ice and 50ul of samples and 50 ul of luciferase reagent were mixed in a 96 well opaque plate. Luminescence was immediately measure on the Flex Station 3. Analysis was performed by back calculation to the standard curve, background subtraction and normalization to live cell controls.

Glycerol-3-phosphate and creatine were measured based on manufacturers' protocols (Abcam). Briefly, supernatants were taken from specified culture conditions and spun at 500 x g. 50 μl of supernatant was added to a 96 well plate. Detection reagents were prepared as indicated in protocol and added to respective wells. Samples were incubated for 40 minutes or 1 hr. for glycerol-3-phosphate and creatine, respectively. OD at 450nm or fluorescence at Ex/Em 535/587 was measured for glycerol-3-phosphate and creatine, respectively.

Flow cytometry of apoptosis and Panx1 activation

Apoptotic cells were stained with Annexin V-Pacific Blue, 7AAD, and TO-PRO-3 for 15 minutes at room temperature in the Annexin V binding buffer (140 mM NaCl, 2.5 μM CaCl, 10 mM HEPES) and subjected to flow cytometry on Attune NxT (Invitrogen). Data were analyzed using FlowJo V10 Software.

Metabolomics analysis of apoptotic supernatant and cell pellet

Sample extraction, processing, compound identification, curation and metabolomic analyses were carried out at Metabolon Inc. (Durham, NC) and Human Metabolome Technologies America (HMT) (Boston, MA) [30]. Briefly, supernatants were separated from cell pellets via sequential centrifugation and frozen before shipment for metabolomic analysis. For HMT; supernatant samples were spiked with 10ul of water with internal standards, then filtered through a 5-kDa cut-off filter to remove macromolecules and small vesicles. Cationic compounds were diluted and measured using positive ion mode ESI via CE-TOFMS. Anionic compounds were measures in the positive or negative ion mode ESI using CE-MS/MS. Samples were diluted to improve the CE-QqQMS analysis. Peak identification and metabolite quantification were determined using migration time, mass to charge ratio, and the peak area normalized to the internal standard and standard curves. Concentrations reported are on a per million cell basis which was derived by back calculations on the cell number that was used in the experimental set-up.

For untargeted metabolomics analysis through Metabolon, recovery standards were added to samples in order to monitor QC of the analysis. Samples were methanol precipitated under shaking for 2 minutes. After, samples were placed on the TurboVap to remove organic solvent and the samples were stored O/N under nitrogen. Samples were analyzed under 4 different conditions; two for analysis by two separate reverse phase (RP)/UPLC-MS/MS methods with positive ion mode ESI, one for analysis by RP/UPLC-MS/MS with negative ion mode ESI, and one for analysis by HILIC/UPLC-MS/MS with negative ion mode ESI. Using a library based on authenticated standards that contains the retention time/index (RI), mass to charge ratio (*m/z*), and chromatographic data (including MS/MS spectral data) on all molecules in the library (Metabolon), the metabolite identification could be performed with reverse scores between the experimental data and authenticated standards. While there may be similarities based on one of these factors, the use of all three data points can be used to identify biochemicals. R code used for heatmap generation and volcano plots is available upon request.

Metabolite flux experiments with ^{13}C-arginine labeling

Cells were re-suspended in arginine free RPMI media containing 10% dialyzed serum, supplemented with 1mM 13C6 L-Arginine HCl (Thermo Fischer Scientific). Cells were either exposed to UV or left untreated. This step was performed within a minute of adding the media containing ^{13}C-arginine to cells. The cells were then incubated at 37 °C. Samples were collected every hour to trace the incorporation of the label from arginine into the polyamine pathway for both UV exposed and live cells. Where indicated, the cells were pre-treated with zVAD-FMK to inhibit caspases.

Metabolite extraction from the pellet or supernatant was performed by adding 300ul of 6%TCA to a pellet of 4 million cells on ice. The samples were then vortexed thoroughly at 4°C, followed by centrifugation to remove cell debris. 100ul of the supernatant and 900ul of Na2Co3 (0.1M, pH 9.3) were mixed, followed by the addition of 25ul of isobutyl chloroformate. The mixture was incubated at 37 °C for 30 minutes and then centrifuged for 10 minutes at 20000g. 800ul of the supernatant was transferred to a fresh tube, followed by the addition of 1000µl of diethyl ether and vortexing. The mixture was allowed to sit at RT for 10 minutes for phase separation after which, 900µl sample was collected in a fresh Eppendorf tube. The samples were dried via Speedvac. For LC-MS runs, 150ul of 1:1 mixture of 0.2% acetic acid in water and 0.2% of acetic acid in acetonitrile was added to the dried sample.

RNA-sequencing

LR73 cells (ATCC) were plated at ($100x10^3$) per well in 24-well tissue culture plates and cultured for 16 hours at 37 °C with 5% CO_2. The cells were then rinsed with phosphate buffered saline (PBS), and fresh supernatants taken from live Jurkat, apoptotic Jurkat (UV), or Panx1-DN apoptotic Jurkat (UV) cells were added for 4 hours (as described above). Total RNA was harvested using the Nucleospin RNA kit (Macherey-Nagal) and an mRNA library was constructed with Illumina TruSeq platform. Transcriptome sequencing using an Illumina NextSeq 500 cartridge was then performed on samples from four independent experiments. RNAseq data was analyzed using Rv1.0.136 and the R package DeSeq2 for

differential gene expression, graphical representation, and statistical analysis. R code used for bioinformatic analysis and heatmap generation is available upon request.

Quantitative RT-PCR analysis

RNA was extracted from cells treated with different live or apoptotic supernatants. Where indicated, supernatants were filtered through a 3kDa filter as suggested by manufacturers' protocol. Briefly, supernatants were separated from cells and large vesicles via sequential centrifugations. Supernatants were then added to 3kDA filters (Millipore) and centrifuged for one hour at 3000 x g prior to adding supernatant to live LR73 cells. Nucleospin RNA kit (Macherey-Nagel) was used for RNA extraction and cDNA was synthesized using QuantiTect Reverse Transcription Kit (Qiagen). Gene expression of indicated genes was performed using Taqman probes (Applied Biosystems) and the StepOnePlus Real Time PCR System (Applied Biosystems).

In-vivo thymocyte death induction

Six- to eight-week old *Panx1*$^{fl/fl}$ or *Panx1*$^{fl/fl}$*Cd4*-Cre mice were injected intraperitoneally with dexamethasone (250 μg). Thymus was harvested 6 hours post-injection and single cell suspension was prepared using 70-μm strainers (Fisher). An aliquot of digested tissue was taken to measure the extent of thymocyte cell death and Pannexin1 activation using Annexin V-Pacific Blue, 7AAD, and TO-PRO-3, as described above. Samples were acquired on Attune NxT (Invitrogen) and analyzed using FlowJo v10 Software.

Thymic myeloid cell isolation and gene expression

Six- to eight-week old *Panx1*$^{fl/fl}$ or *Panx1*$^{fl/fl}$*Cd4*-Cre mice were injected with dexamethasone and single cell suspensions of thymus were prepared as described above. Following isolation, cells were incubated with anti-CD16/CD32 (Fc-Block, Invitrogen) for 20 minutes at 4°C. Cells were then stained with anti-CD3-PE and run through a MACS kit using anti-PE microbeads to 'de-bulk' the cell suspension and remove a majority of thymocytes. Cell flow through (CD3neg population) was collected and then stained with anti-CD11b-PE and anti-CD11c-PE antibodies 30 minutes at 4°C. Stained cells were purified using the anti-PE MicroBeads MACS kit (Miltenyi Biotec), following manufacturers protocol. Sample aliquots were run on the Attune NxT (Invitrogen) and analyzed using FlowJo v10 Software. Total RNA from purified cells was isolated Nucleospin RNA kit (Macherey-Nagel) for cDNA synthesis and qRT-PCR, as described above.

Memix preparation and in vivo treatment

The metabolite mixture *MeMix*[6] was composed of these six metabolites: spermidine, fructose 1,6-bisphosphate (FBP), dihydroxyacetone phosphate (DHAP), guanosine 5'-monophosphate (GMP), inosine 5'-monophosphate (IMP), and UDP-glucose. *MeMix*[3] was composed of spermidine, GMP and IMP. Concentrations of metabolites used for *in vitro* LR73 phagocyte treatment were as follows (based on targeted metabolomics): IMP (3.3μM), DHAP (36μM), FBP (0.5μM), GMP (2.1μM), UDP-Glucose (2μM), Spermidine (0.3μM). Concentration of metabolites used for *in vivo* mice treatment were as follows: IMP (100mg/

kg), DHAP (50mg/kg), FBP (500mg/kg), GMP (100mg/kg), UDP-Glucose (100mg/kg), Spermidine (100mg/kg).

K/BxN induced arthritis

C57BL/6J mice were given intraperitoneal injections of 150 μl of serum from K/BxN mice on day 0 and paw swelling was measured at indicated time points using a caliper (Fisher). Measurements are presented as percent change from day 0. On day 1, mice were randomly assigned into three groups and given daily intraperitoneal injections of either *MeMix*$^{(3or6)}$ or vehicle through day 5. In separate experiments, mice on day 1 were randomly assigned and given daily injections of either live or apoptotic supernatants through day 5. Clinical scores were assigned for each paw as follows: 0 – no paw swelling or redness observed, 1 – redness of the paw or a single digit swollen, normal V shape of the hind foot (the foot at the base of the toes is wider than the heel and ankle) 2 – two or more digits swollen or visible swelling of the paw, U shape of the hind foot (the ankle and the midfoot are equal in thickness), 3 – reversal of the V shape of the hind foot into an hourglass shape (the foot is wider at the heel than at the base of the toes). A combined clinical score of all paws is presented. Paw measurements and clinical score assignments were performed by an investigator blinded to the treatment groups.

Lung Transplant Rejection Model

Orthotopic left lung transplantation was carried out according to previous reports. To study the alteration of allo-immune response by a minor antigen-mismatched combination, C57BL/10 donor and C57BL/6 recipients were used. The recipient mice were administrated with *MeMix*^{3} or vehicle intraperitoneally on post-operative Day 1 and Day 3. On Day 7, the recipient mice were sacrificed and left lung allografts were harvest and processed for histology.

Histology

Lungs were fixed in formalin, sectioned, and stained with hematoxylin and eosin (H&E). The acute rejections were graded according to the International Society for Heart and Lung Transplantation (ISHLT) A Grade criteria by a lung pathologist who is blinded to the experimental settings[28]. For arthritis mice were euthanized at day 8 of K/BxN serum induced arthritis and the hind paws were fixed in 10% formalin (Fisher). Decalcification, sectioning, paraffin embedding, hematoxylin and eosin (H&E) staining and Safranin O staining was performed by HistoTox Labs (Boulder, CO). Images of ankle sections were taken on an EVOS FL Auto (Fisher) and analyzed using the accompanying software. Histology scoring was performed by an investigator blinded to the mouse treatment. For inflammation and cartilage erosion scoring, the following criteria were used - 0, none; 1, mild; 2, moderate; 3, severe. For bone erosion scoring, the following criteria were used: 0, no bone erosions observed; 1, mild cortical bone erosion; 2, severe cortical bone erosion without the loss of bone integrity; 3, severe cortical bone erosion with the loss of cortical bone integrity and trabecular bone erosion.

Statistical analysis

Statistical significance was determined using GraphPad Prism 7, using unpaired Student's two-tailed *t*-test (paired and unpaired), one-way ANOVA, or two-way ANOVA according to test requirements. Grubbs' Outlier Test was used to determine outliers, which were excluded from final analysis. A p value of <.05 (indicated by one asterisk), <.01 (indicated by two asterisks), <.001 (indicated by three asterisks), or <.0001 (indicated by four asterisks) were considered significant.

Extended Data

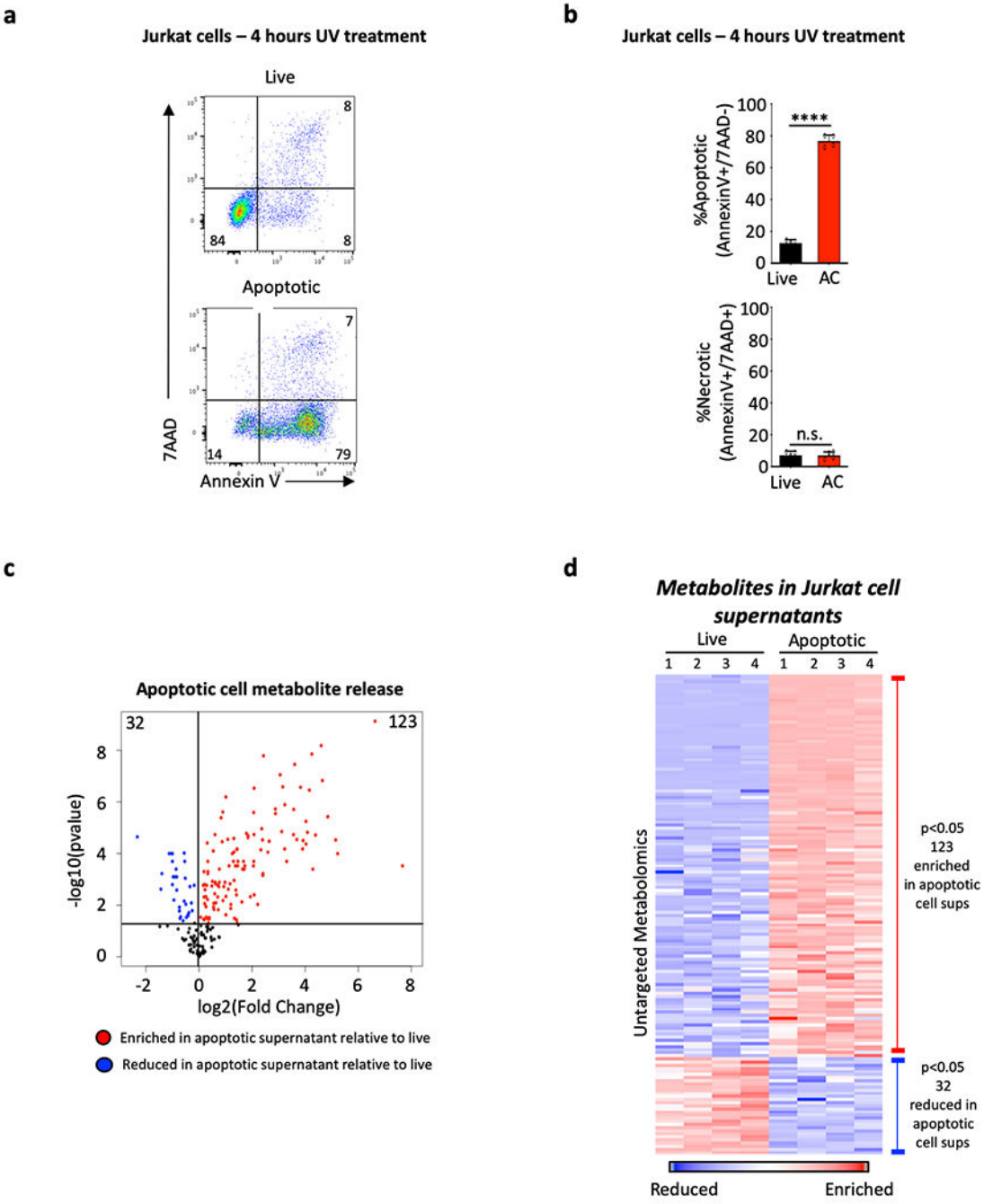

Extended Data 1. Metabolite release from apoptotic Jurkat cells

a, Jurkat cells were induced to undergo apoptosis after UV irradiation. Staining with 7AAD and Annexin V (AV) were used to determine the percentage of live ($AV^{-}7AAD^{-}$), apoptotic ($AV^{+}7AAD^{-}$), or necrotic ($AV^{+}7AAD^{+}$) cells after 4 hours. **b,** Quantitative analysis of apoptosis (top) and secondary necrosis (bottom) (n=4). Data are mean ± s.d. Unpaired two-tailed Student's t-test. **** p< .0001. **c,** Volcano Plot produced from untargeted metabolomics of Jurkat T cell supernatants representing statistically enriched or reduced (p < .05) metabolites in the apoptotic supernatants relative to live supernatant. Data are

representative of four biological replicates. Two-sided Welch's two-sample t-test. **d,** Heatmap produced from untargeted metabolomics of Jurkat T cell supernatants representing statistically enriched or reduced ($p < .05$) metabolites in the apoptotic supernatants relative to live supernatants. Data are representative of four biological replicates. Two-sided Welch's two-sample t-test.

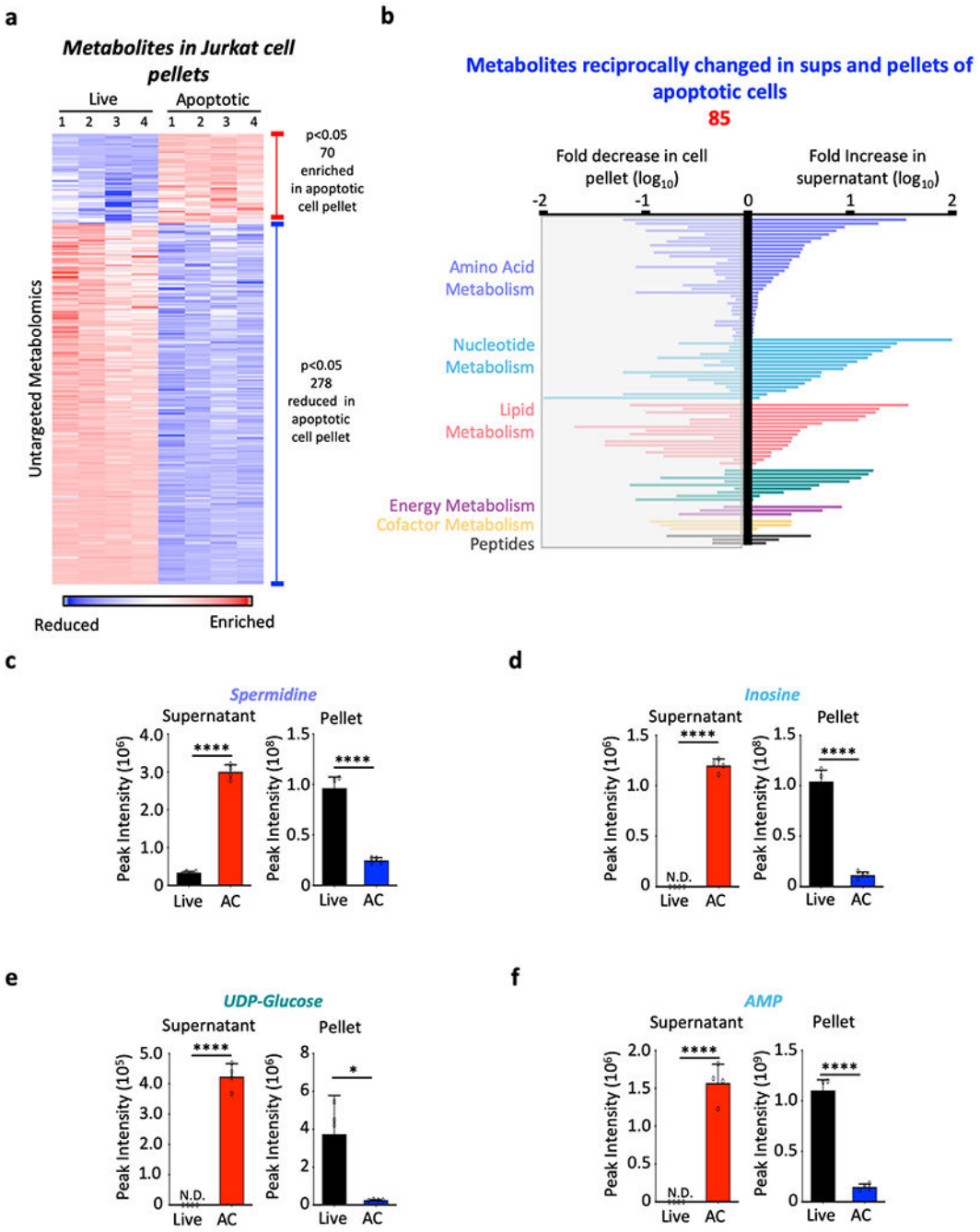

Extended Data 2. Reciprocal metabolite changes between apoptotic supernatant and pellet

a, Heatmap produced from untargeted metabolomics of Jurkat T cell pellets representing statistically enriched or reduced ($p < .05$) metabolites in the apoptotic pellet relative to live cell pellet (n=4 biologically independent samples). Two-sided Welch's two-sample t-test. **b,** Bi-directional plot representing the 85 metabolites that were statistically enriched in the apoptotic supernatant ($p < .05$) and simultaneously reduced in the apoptotic cell pellet relative to live cell conditions. Metabolites were grouped by metabolic pathways (n=4 biologically independent samples). Two-sided Welch's two-sample t-test. **c-f,** Mass

spectrometry was used to determine the relative amount of (c) spermidine. (**** p< .0001), (d) inosine (**** p< .0001), (e) UDP-glucose (supernatant **** p< .0001, pellet *p=0.014), and (f)AMP (**** p< .0001) in Jurkat T cell supernatants and cell pellets in live and apoptotic conditions (n=4 biologically independent samples). Data are mean ± s.d. Unpaired two-tailed Student's t-test.

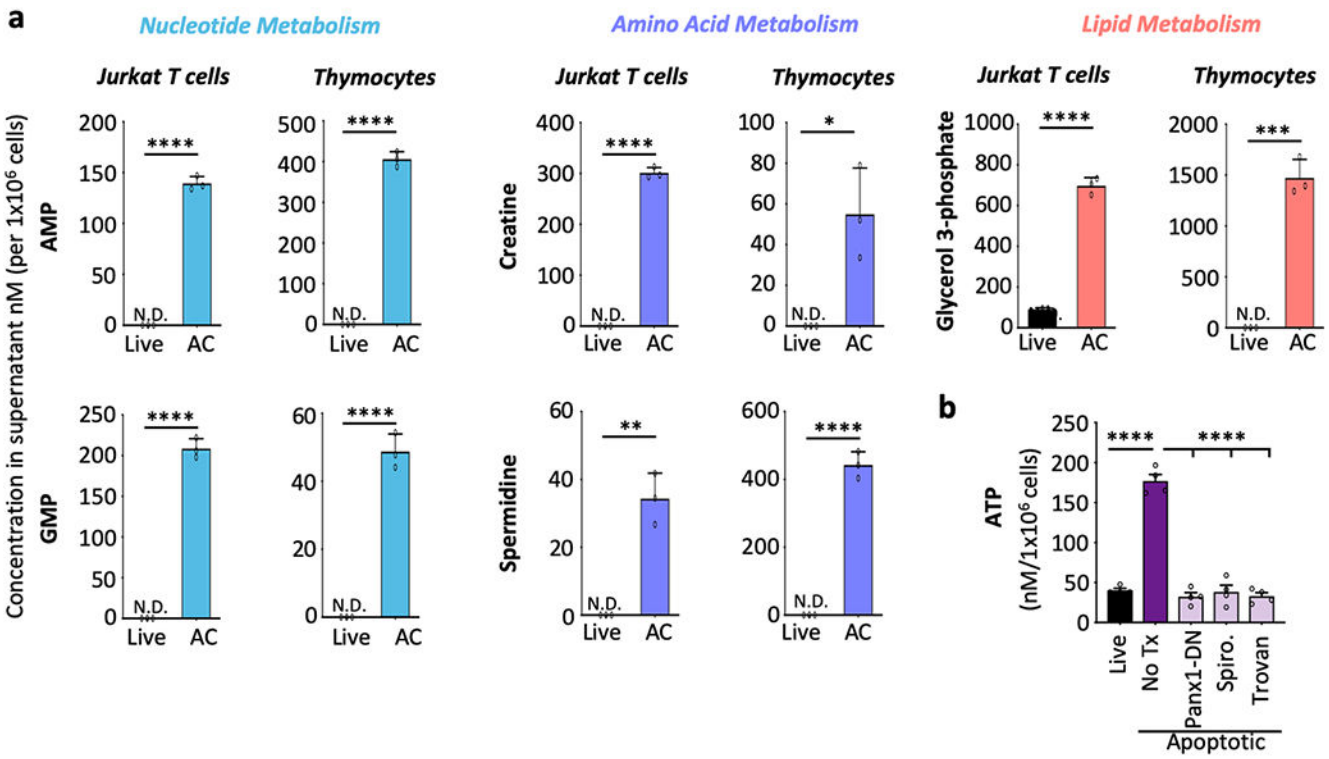

c

Cell Type	Apoptotic Stimulus	Approach	Metabolites Screened
1. Jurkat E6.1 (T cell)	UV	Untargeted Metabolomics	>3000
	Fas	Targeted Metabolomics	116
	ABT-737 (BH3 mimetic)	Colorimetric/Fluorometric Kit	ATP, Spermidine
2. Primary Thymocyte	Fas	Targeted Metabolomics	116
3. Primary BMDM	Anthrax Lethal Toxin	Untargeted Metabolomics	>3000
4. A549 (Lung epithelial cell)	UV	Colorimetric/Fluorometric Kit	ATP, Spermidine, G-3-P, Creatine
	ABT-737 (BH3 mimetic)	Colorimetric/Fluorometric Kit	ATP, Spermidine, G-3-P, Creatine
5. HCT116 (colonic epithelial cell)	ABT-737 (BH3 mimetic)	Colorimetric/Fluorometric Kit	ATP, Spermidine, G-3-P, Creatine
	TRAIL	Colorimetric/Fluorometric Kit	ATP, Spermidine, G-3-P, Creatine

Extended Data 3. Conserved metabolite release during apoptosis

a, Mass spectrometry was used to measure the concentration of the of the five metabolites that were released across all conditions and platforms tested in live or apoptotic supernatants per million Jurkat T cells (left) or isolated primary thymocytes (right) (back-calculated from total cells used in experimental set-up) (n=3). Metabolites are grouped by pathways to which they have been linked. Data are mean ± s.d. Unpaired two-tailed Student's t-test. Thymocyte-creatine *p=0.014, Jurkat-spermidine **p=0.0014, Thymocyte-glycerol-3-phosphate ***p=0.0002, **** p < .0001. **b,** Luciferase assay was used to measure the concentration of ATP release in the supernatant across the different apoptotic Jurkat cells

(n=4). Data are mean ± s.e.m. Ordinary One-way ANOVA, Turkey's multiple comparison test. **** p < .0001. **c,** Table outlining the different cell types, apoptotic stimulus, techniques and metabolites screened for Untargeted (>3000 features/compounds) and Targeted (116 metabolites) metabolomics included ATP, Spermidine, Glycerol-3-phosphate (G-3-P) and creatine.

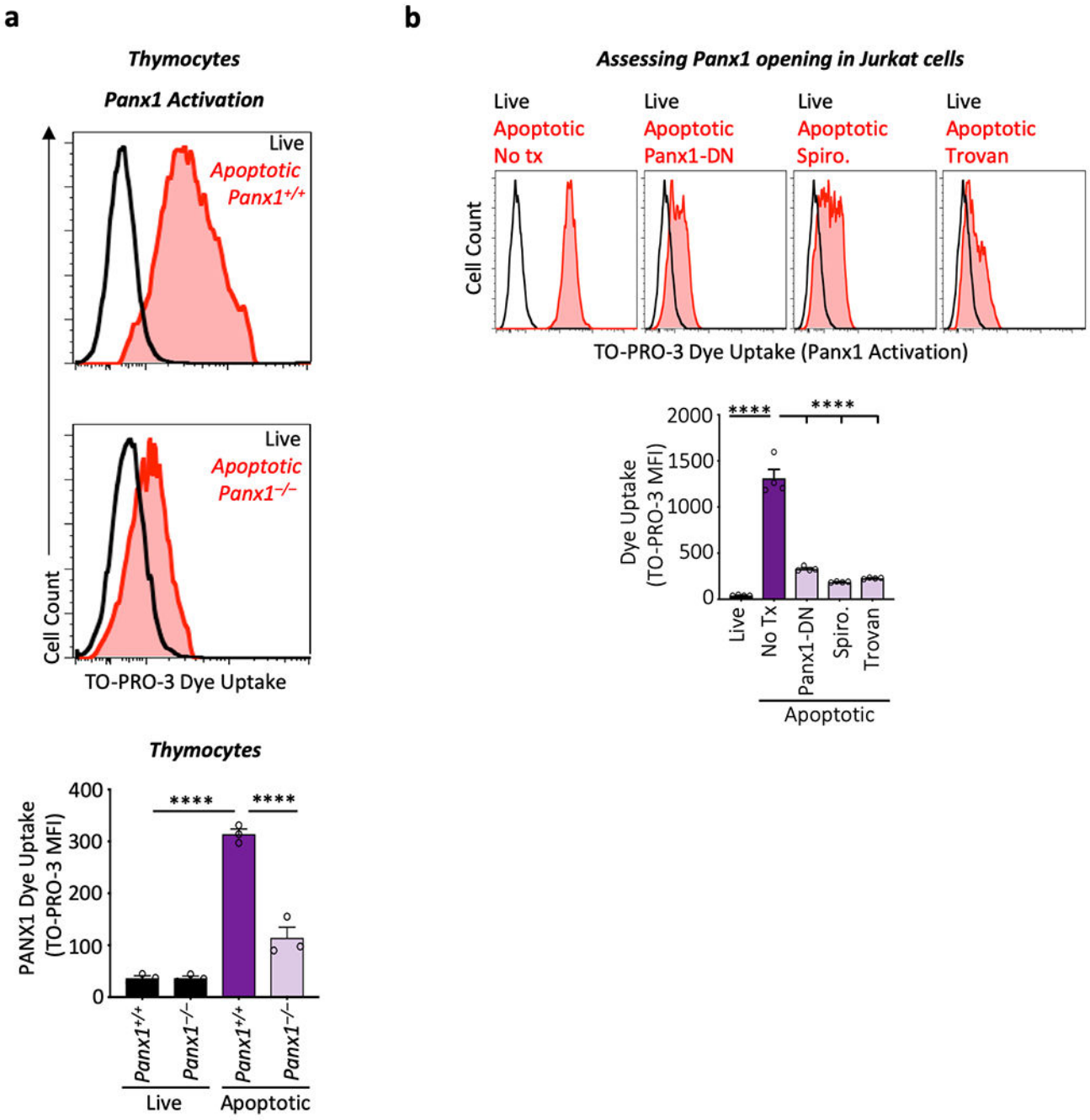

Extended Data 4. Panx1 activation and inhibition during cell death

a, Representative histograms of TO-PRO-3 dye uptake (top) as a readout of Panx1 activation in live and apoptotic thymocytes from wild type ($Panx1^{+/+}$) and Panx1 knockout ($Panx1^{-/-}$) mice. Quantification of Panx1 activation across different conditions was assessed via flow cytometry by measuring the mean fluorescent intensity of TO-PRO-3 dye uptake (bottom) (n=3). Data are mean ± s.e.m. Ordinary One-way ANOVA, Turkey's multiple comparison test. **** p <.0001. **b,** Representative histograms of TO-PRO-3 dye uptake as a readout of Panx1 activation in live and apoptotic wild-type Jurkat T cells, Panx1-DN Jurkat T cells, and

Jurkat T cells treated with two different Panx1 inhibitors spironolactone (50μM) or trovafloxacin (25μM) (top). Quantification of TO-PRO-3 dye uptake by the apoptotic cells measured as MFI assessed using flow cytometry (bottom) (n=4). Data are mean ± s.e.m. Ordinary One-way ANOVA, Turkey's multiple comparison test. **** $p < .0001$.

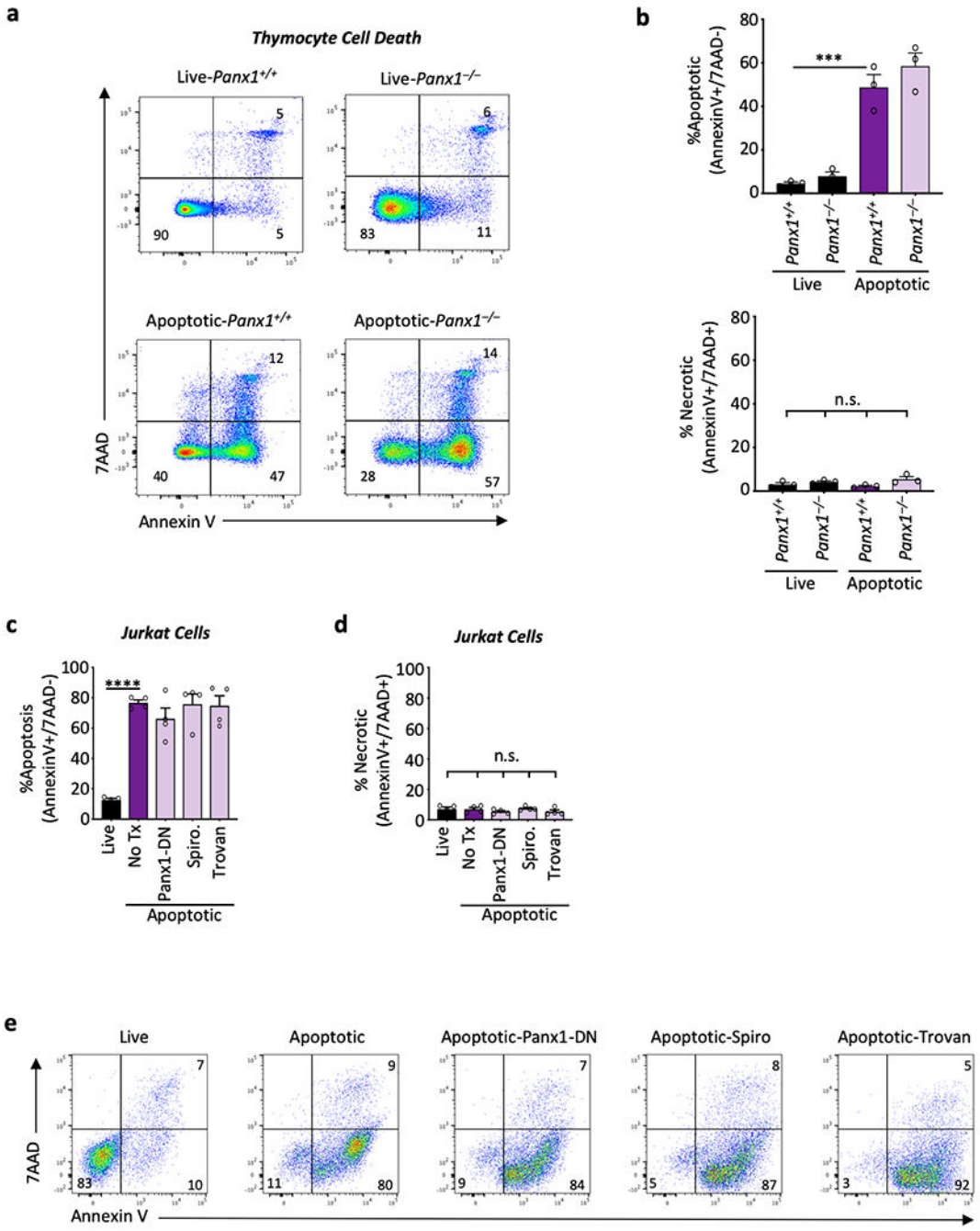

Extended Data 5. Panx1 inhibition does not influence apoptotic cell death

a, Control or Panx1$^{-/-}$thymocytes were treated with anti-Fas (5μg ml^{-1}) for 1.5 hours. Cells were stained with 7AAD and Annexin V to determine the percentage of live (AV^{-}7AAD^{-}), apoptotic (AV^{+}7AAD^{-}), or necrotic (AV^{+}7AAD^{+}) cells. **b,** Quantitation of apoptosis (top) and secondary necrosis (bottom) of control and Panx1 knockout thymocytes (n=3). Data are mean ± s.e.m. Ordinary One-way ANOVA, Turkey's multiple comparison test. ***p=0.0004. **c,d,** Quantification of apoptosis and secondary necrosis from the samples prior to metabolomics analysis (n=4). Data are mean ± s.e.m. Ordinary One-way ANOVA,

Turkey's multiple comparison test. ****p < .0001. **e,** Cells were stained with 7AAD and Annexin V to determine the percent of live ($AV^{-}7AAD^{-}$), apoptotic ($AV^{+}7AAD^{-}$), or necrotic ($AV^{+}7AAD^{+}$) cells.

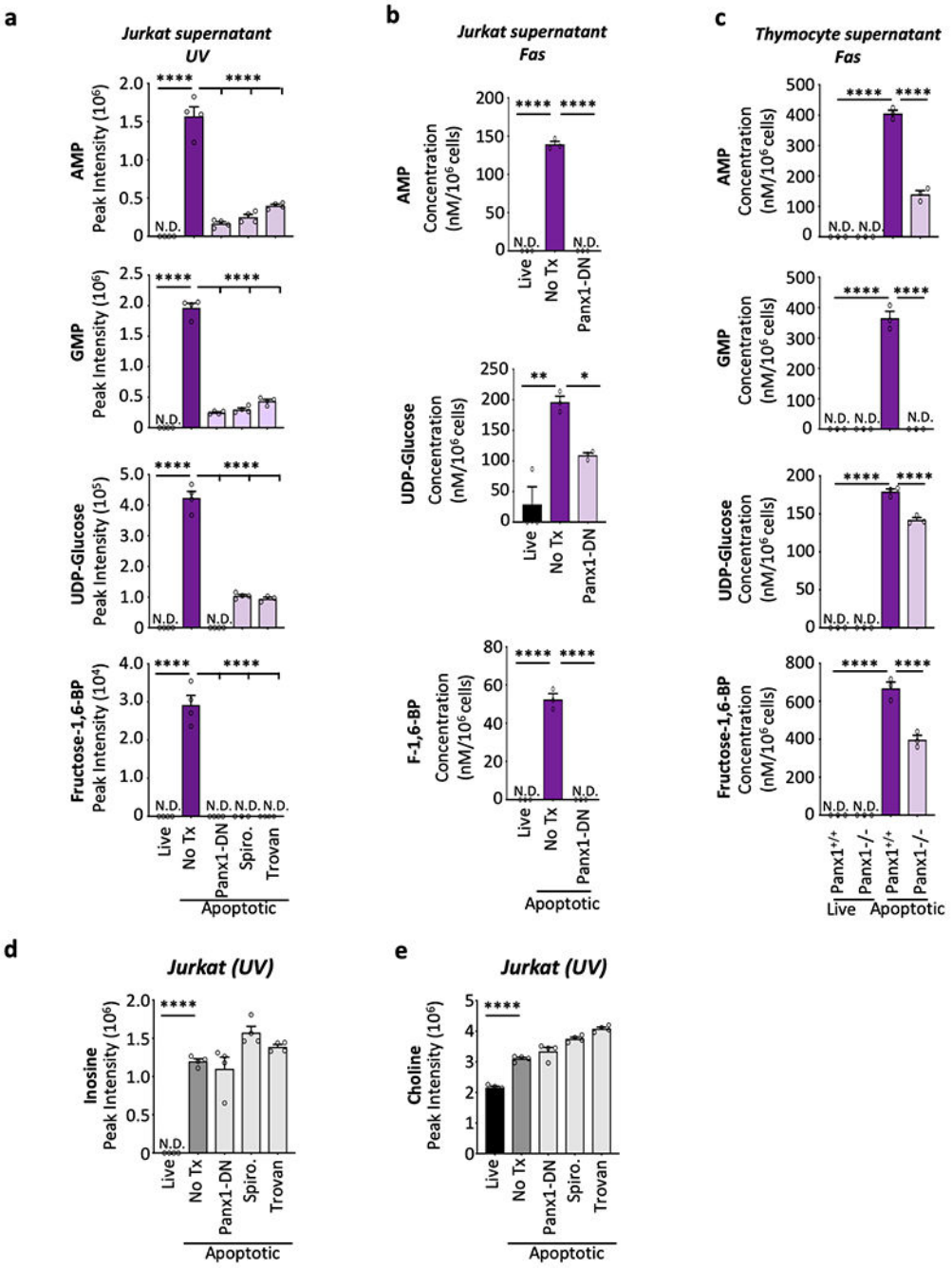

Extended Data 6. Panx1-dependent metabolite release during apoptosis

a, Mass spectrometry was used to determine the relative amount of AMP, GMP, UDP-Glucose, and fructose 1,6-bisphosphate in Jurkat T cell supernatant across different conditions (n=4). Data are mean ± s.e.m. Ordinary One-way ANOVA, Turkey's multiple comparison test. **** $p < .0001$. **b,** Jurkat cells were induced to undergo apoptosis with anti-Fas treatment (250ng ml^{-1}). Mass spectrometry was used to measure the absolute concentration per million cells of (a) AMP, (b) UDP-glucose, and (c) fructose 1,6-bisphosphate in the supernatants of Jurkat T cells across different conditions (back-

calculated from total cells used in experimental set-up) (n=3). Data are mean ± s.e.m. Ordinary One-way ANOVA, Turkey's multiple comparison test. (UDP-Glucose Live vs. No Txn **p=0.0013, No Txn vs. Panx1-DN *p=0.031, **** p< .0001). **c,** Mass spectrometry was used to determine the absolute concentration of AMP, GMP, UDP-Glucose, and fructose 1,6-bisphosphate per million cells (back-calculated from total cells used in experimental set-up) in the supernatant from isolated primary thymocytes across different conditions (n=3). Data are mean ± s.e.m. Ordinary One-way ANOVA, Turkey's multiple comparison test. **** p< .0001. **d-e,** Relative concentrations were determined by mass spectrometry for inosine (d) and choline (e) in live, apoptotic, or apoptotic supernatants where Panx1 was inhibited (n=4). Data are mean ± s.e.m. Ordinary One-way ANOVA, Turkey's multiple comparison test. **** p<.0001.

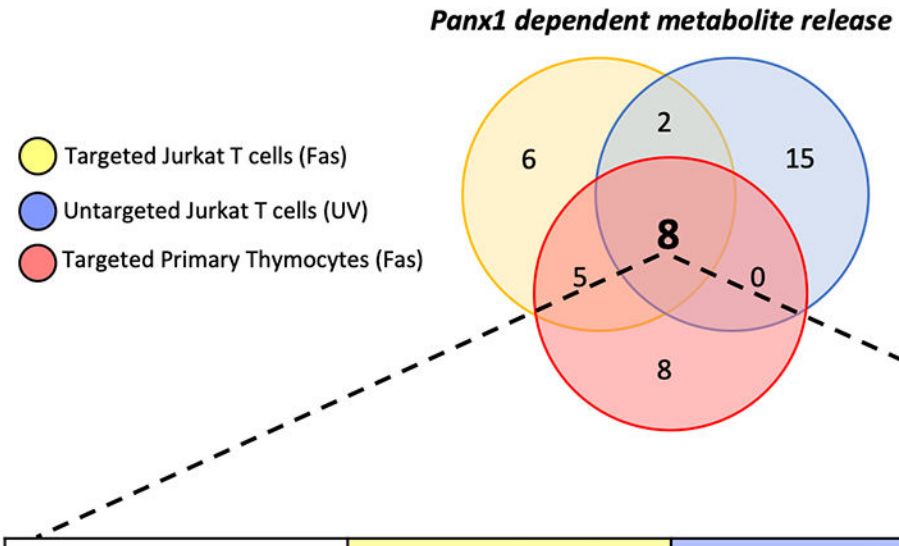

Panx1-depenedent metabolites (Consistent across all platforms/conditions)	Targeted (Jurkat) (nM/10^6 cells)			Untargeted (Jurkat) (Peak Intensity)			Targeted (Thymocytes) (nM/10^6 cells)		
	Live	Apoptotic	Apoptotic Px1DN	Live	Apoptotic	Apoptotic Px1DN	Live	Apoptotic Panx1$^{+/+}$	Apoptotic Panx1$^{-/-}$
spermidine	N.D.	34	N.D.	$0.3x10^6$	$3.0x10^6$	$0.8x10^6$	N.D.	441	49
dihydroxyacetone phosphate (DHAP)	N.D.	3559	650	N.D.	$1.2x10^6$	$0.2x10^6$	N.D.	1471	581
Glycerol 3 - phosphate	89	697	359	$0.4x10^6$	$5.4x10^6$	$1.6x10^6$	42	248	166
fructose- 1,6- bisphosphate	N.D.	52	N.D.	N.D.	$2.9x10^4$	N.D.	N.D.	668	397
adenosine 5'-monophosphate (AMP)	N.D.	139	N.D.	N.D.	$1.6x10^6$	$0.2x10^6$	N.D.	406	140
inosine 5'-monophosphate (IMP)	28	330	55	N.D.	$2.2x10^6$	$0.09x10^6$	35	140	84
guanosine 5'-monophosphate (GMP)	N.D.	208	7	N.D.	$2.0x10^6$	$0.2x10^6$	N.D.	52	N.D.
UDP-glucose	87	196	109	N.D.	$4.2x10^5$	$2.5x10^5$	N.D.	182	142

Extended Data 7. Conserved Panx1 secretome

a, Three-way Venn diagram (top) comparing Panx1-dependent metabolites released from apoptotic cells across different conditions tested. Table (bottom) showing the relative peak intensity (untargeted metabolomics) or absolute concentrations (targeted metabolomics) in the supernatant of the indicated cell treatments and knockout mice.

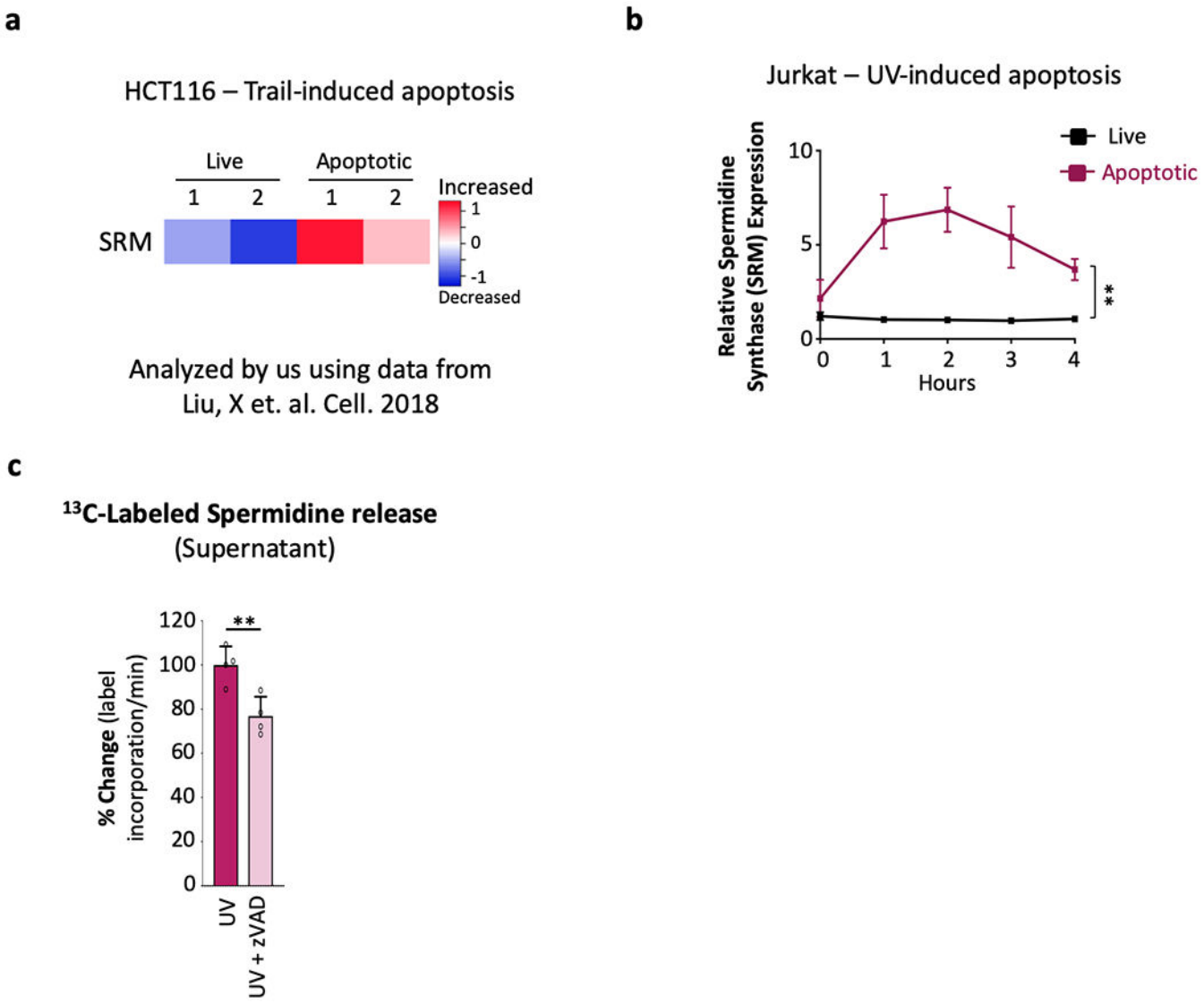

Extended Data 8. Transcriptional and metabolic changes during apoptosis

a, Re-analyses of RNA-seq data from apoptotic cells (Lui et. al., 2018) demonstrating that the SRM mRNA levels are increased/retained during apoptosis. **b,** After induction of apoptosis (n=4), the SRM mRNA expression was assessed over time relative to live controls (n=5). Data are mean ± s.e.m. Two-way ANOVA (**p=0.007). **c,** Incorporation of ^{13}C-labeled arginine into the polyamine pathway intermediate spermidine and release from Jurkat cells after apoptosis, and its partial reduction by the pan-caspase inhibitor zVAD (n=3). Data are mean ± s.d. Unpaired two-tailed Student's t-test (**p=0.0088).

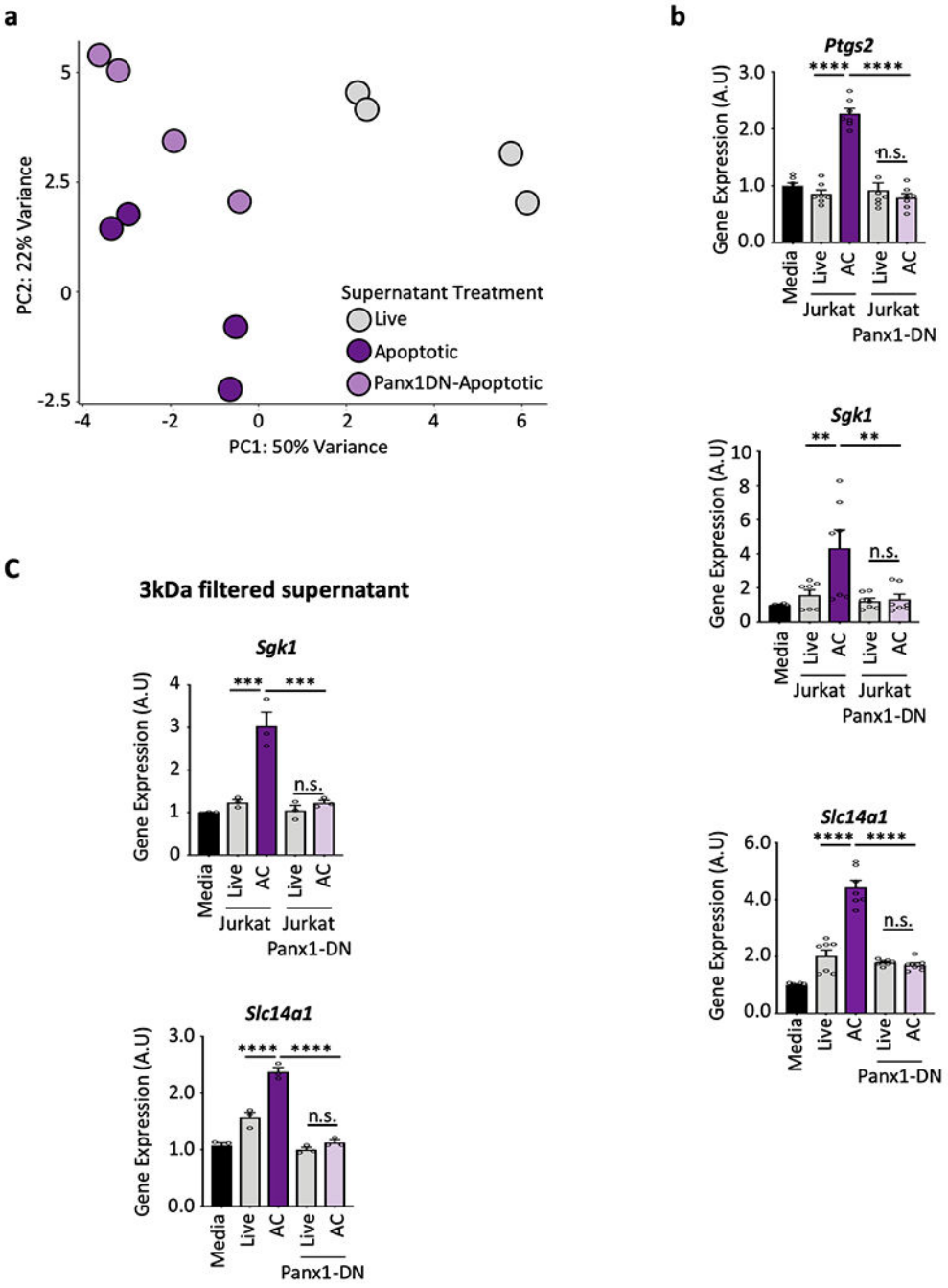

Extended Data 9. Transcriptional changes on surrounding phagocytes induced by Panx1-dependent metabolite release during apoptosis

a, Principle component analysis (PCA) on the RNAseq data as a quality control statistic (n=4 biological replicates). **b,** Experimental procedure was as described in Figure 3d. qPCR was used to assess gene expression changes in *Ptgs2* (top) (****p<0.0001) and *Sgk1* (middle) (Live-AC **p=0.0074, AC-AC-Panx1DN **p=0.0031) (and *Slc14a1* (bottom) (****p<0.0001) in phagocytes after treatment with supernatants from Jurkat cells or Jurkat cells expressing dominant negative Panx1 (n=7). Data are mean ± s.e.m. Ordinary One-way

ANOVA, Turkey's multiple comparison test. **c,** Experimental procedure was as described in Figure 3d, however before treatment of LR73 cells with supernatant, the supernatant was filtered through a 3kDa filter to remove large molecules. qPCR was used to assess gene expression changes in and *Sgk1* (top) (***p=0.0001) and *Slc14a1* (bottom) (****p<0.0001) in phagocytes after treatment with supernatants under specified conditions (n=3). Data are mean ± s.e.m. Ordinary One-way ANOVA, Turkey's multiple comparison test.

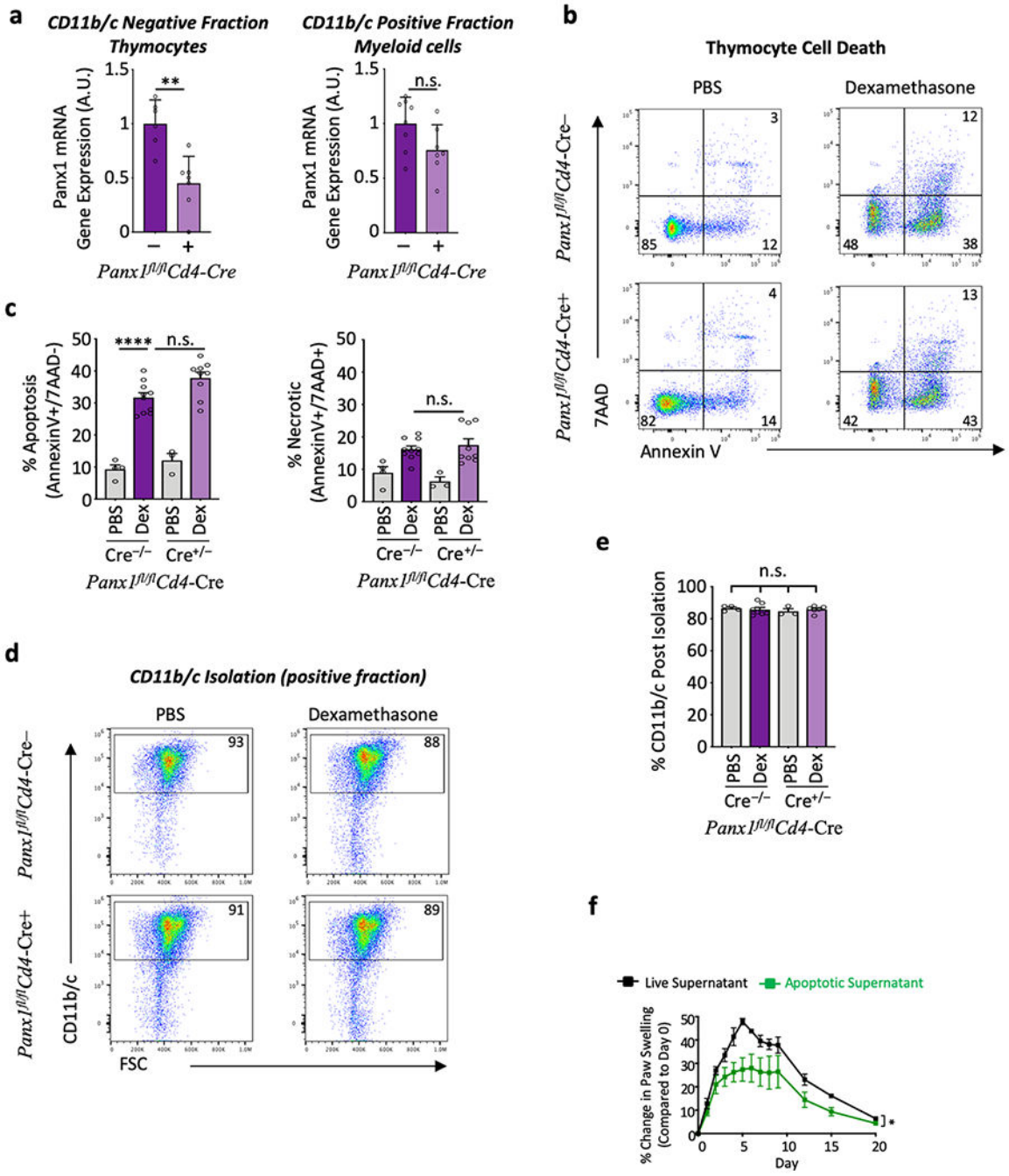

Extended Data 10. In-vivo thymic cell death analysis and supernatant effects during arthritis

a, Analysis of thymic populations used for experimental data presented in Figure 4a. After thymus isolation, the CD11b^{-}CD11c^{-} population which contained thymocytes was used for mRNA isolation to test the efficiency of deletion *Panx1* allele. qPCR analysis of *Panx1* mRNA in wild-type (*Panx1*$^{fl/fl}$ CD4-Cre^{-}) (n=6) or mice in which Panx1 has been knocked out in thymocytes (*Panx1*$^{fl/fl}$ CD4-Cre^{+}) (n=7) (left) (**p=0.0015). CD11b+/c+ myeloid cells harvested from the thymus of *Panx1fl/flCd4-Cre −/+* were analyzed for Panx1 expression to demonstrate that Panx1 not deleted. Panx1 deletion was only deleted from

thymocytes and not the myeloid cells which do not express CD4. Data are mean ± s.d. Unpaired two-tailed Student's t-test. **b,** Representative flow cytometric plots showing the extent of apoptosis induced by dexamethasone in control and *Panx1*$^{fl/fl}$ CD4-Cre^{+} mice. After thymus isolation, an aliquot of cells was stained with 7AAD and Annexin V to determine the % of live, apoptotic, or necrotic (AV^{+}7AAD^{+}) cells. **c,** Quantitative analysis of apoptosis (left) and secondary necrosis (right) of CD11b^{-}CD11c^{-} thymic populations from *Panx1*$^{fl/fl}$ CD4-Cre^{-} (PBS n=4, Dex n=10) or *Panx1*$^{fl/fl}$ CD4-Cre^{+} (PBS n=3, Dex n=9) mice treated with PBS or dexamethasone. Data are mean ± s.e.m. Ordinary One-way ANOVA, Turkey's multiple comparison test (****p<0.0001). **d,** Representative flow cytometry plots demonstrating the purity of CD11b^{+}CD11c^{+} population after magnetic separation from the different mice and treatment conditions. **e,** Comparison of the CD11b+CD11c+ cells isolated from the different conditions. *Panx1*$^{fl/fl}$ CD4-Cre^{-} (PBS n=4, Dex n=7) or *Panx1*$^{fl/fl}$ CD4-Cre^{+} (PBS n=3, Dex n=6). Data are mean ± s.e.m. Ordinary One-way ANOVA, Turkey's multiple comparison test. **f,** Apoptotic supernatants alleviate KBx/N induced arthritic disease. C57Bl/6J mice were injected with K/BxN serum to induce arthritis. Live (n=4) or apoptotic (n=5) supernatant was given for five days after arthritis induction. Paw swelling was measured using a caliper and reported as % change compared to day 0. Data are mean ± s.e.m. Two-way ANOVA (*p=0.0131).

Supplementary Material

Refer to Web version on PubMed Central for supplementary material.

Acknowledgements

The authors thank members of the Ravichandran laboratory, and members of the Pannexin Interest Group at UVA for numerous discussions, and critical reading of the manuscript. This work is supported by grants to K.S.R. from NHLBI (P01HL120840), NIGMS R35GM122542, and the Center for Cell Clearance/University of Virginia School of Medicine, and the Odysseus Award from the FWO, Belgium, EOS Grant from the FWO (3083753-DECODE), and the NHLBI (P01HL120840) and NIAID (R21 AI139967 and R21 AI135455) to U.L. Additional support was received through the NIH T32 Pharmacology Training Grant (T32GM007055) (C.B.M, and B.B.), Mark Foundation Fellowship from the Cancer Research Institute and a K99 from the NCI (to J.S.A.P.), and the Kanye Foundation of Japan (to S.M.). Current address for Justin Perry: Immunology Program, Memorial Sloan-Kettering Cancer Center, New York, NY.

References

1. Fuchs Y & Steller H Programmed cell death in animal development and disease. Cell 147, 742–758 (2011). [PubMed: 22078876]
2. Rothlin CV, Carrera Silva EA, Bosurgi L & Ghosh S TAM receptor signaling in immune homeostasis. Annu. Rev. Immunol. 33, 355–391 (2015). [PubMed: 25594431]
3. Lindsten T et al. The combined functions of proapoptotic Bcl-2 family members bak and bax are essential for normal development of multiple tissues. Mol. Cell 6, 1389–1399 (2000). [PubMed: 11163212]
4. Gregory CD, and Pound JD Cell death in the neighbourhood: direct microenvironmental effects of apoptosis in normal and neoplastic tissues. J. Pathol. 223, 177–194 (2011). [PubMed: 21125674]
5. Ryoo HD, Gorenc T & Steller H Apoptotic cells can induce compensatory cell proliferation through the JNK and the Wingless signaling pathways. Dev. Cell 7, 491–501 (2004). [PubMed: 15469838]
6. Ke FFS et al. Embryogenesis and Adult Life in the Absence of Intrinsic Apoptosis Effectors BAX, BAK, and BOK. Cell 173, 1217–1230.e17 (2018). [PubMed: 29775594]

7. Medina CB & Ravichandran KS Do not let death do us part: ‘find-me’ signals in communication between dying cells and the phagocytes. Cell Death Differ. 23, 979–989 [PubMed: 26891690]
8. Elliott MR et al. Nucleotides released by apoptotic cells act as a find-me signal to promote phagocytic clearance. Nature 461, 282–286 (2009). [PubMed: 19741708]
9. Van Opdenbosch N et al. Caspase-1 Engagement and TLR-Induced c-FLIP Expression Suppress ASC/Caspase-8-Dependent Apoptosis by Inflammasome Sensors NLRP1b and NLRC4. Cell Rep 21, 3427–3444 (2017). [PubMed: 29262324]
10. Chekeni FB et al. Pannexin 1 channels mediate ‘find-me’ signal release and membrane permeability during apoptosis. Nature 467, 863–867 (2010). [PubMed: 20944749]
11. Poon IKH et al. Unexpected link between an antibiotic, pannexin channels and apoptosis. Nature 507, 329–334 (2014). [PubMed: 24646995]
12. Good ME et al. Pannexin 1 Channels as an Unexpected New Target of the Anti-Hypertensive Drug Spironolactone. Circ. Res. 122, 606–615 (2018). [PubMed: 29237722]
13. Madeo F, Eisenberg T, Pietrocola F & Kroemer G Spermidine in health and disease. Science 359, eaan2788 (2018). [PubMed: 29371440]
14. Liu X et al. PNPT1 Release from Mitochondria during Apoptosis Triggers Decay of Poly(A) RNAs. Cell (2018). doi:10.1016/j.cell.2018.04.017
15. Morioka S et al. Efferocytosis induces a novel SLC program to promote glucose uptake and lactate release. Nature 16, 907 (2018).
16. Wang Y et al. Mitochondrial Fission Promotes the Continued Clearance of Apoptotic Cells by Macrophages. Cell 171, 331–345.e22 (2017). [PubMed: 28942921]
17. Perry JSA et al. Interpreting an apoptotic corpse as anti-inflammatory involves a chloride sensing pathway. Nat. Cell Biol. 21, 1532–1543 (2019). [PubMed: 31792382]
18. Ipseiz N et al. The nuclear receptor Nr4a1 mediates anti-inflammatory effects of apoptotic cells. J. Immunol. 192, 4852–4858 (2014). [PubMed: 24740500]
19. Chung EY et al. Interleukin-10 expression in macrophages during phagocytosis of apoptotic cells is mediated by homeodomain proteins Pbx1 and Prep-1. Immunity 27, 952–964 (2007). [PubMed: 18093541]
20. Zaiss DMW, Gause WC, Osborne LC & Artis D Emerging functions of amphiregulin in orchestrating immunity, inflammation, and tissue repair. Immunity 42, 216–226 (2015). [PubMed: 25692699]
21. Goessling W et al. Genetic interaction of PGE2 and Wnt signaling regulates developmental specification of stem cells and regeneration. Cell 136, 1136–1147 (2009). [PubMed: 19303855]
22. Shayakul C, Clémençon B & Hediger MA The urea transporter family (SLC14): physiological, pathological and structural aspects. Mol. Aspects Med. 34, 313–322 (2013). [PubMed: 23506873]
23. Jha AK et al. Network integration of parallel metabolic and transcriptional data reveals metabolic modules that regulate macrophage polarization. Immunity 42, 419–430 (2015). [PubMed: 25786174]
24. Scher JU & Pillinger MH The anti-inflammatory effects of prostaglandins. J. Investig. Med. 57, 703–708 (2009).
25. Korganow AS et al. From systemic T cell self-reactivity to organ-specific autoimmune disease via immunoglobulins. Immunity 10, 451–461 (1999). [PubMed: 10229188]
26. Veras FP et al. Fructose 1,6-bisphosphate, a high-energy intermediate of glycolysis, attenuates experimental arthritis by activating anti-inflammatory adenosinergic pathway. Sci Rep 5, 15171 (2015). [PubMed: 26478088]
27. Krupnick AS et al. Orthotopic mouse lung transplantation as experimental methodology to study transplant and tumor biology. Nat Protoc 4, 86–93 (2009). [PubMed: 19131960]
28. Stewart S et al. Revision of the 1996 working formulation for the standardization of nomenclature in the diagnosis of lung rejection. in 26, 1229–1242 (2007).
29. Kouskoff V et al. Organ-specific disease provoked by systemic autoimmunity. Cell 87, 811–822 (1996). [PubMed: 8945509]
30. Evans AM, DeHaven CD, Barrett T, Mitchell M & Milgram E Integrated, nontargeted ultrahigh performance liquid chromatography/electrospray ionization tandem mass spectrometry platform

for the identification and relative quantification of the small-molecule complement of biological systems. Anal. Chem. 81, 6656–6667 (2009). [PubMed: 19624122]

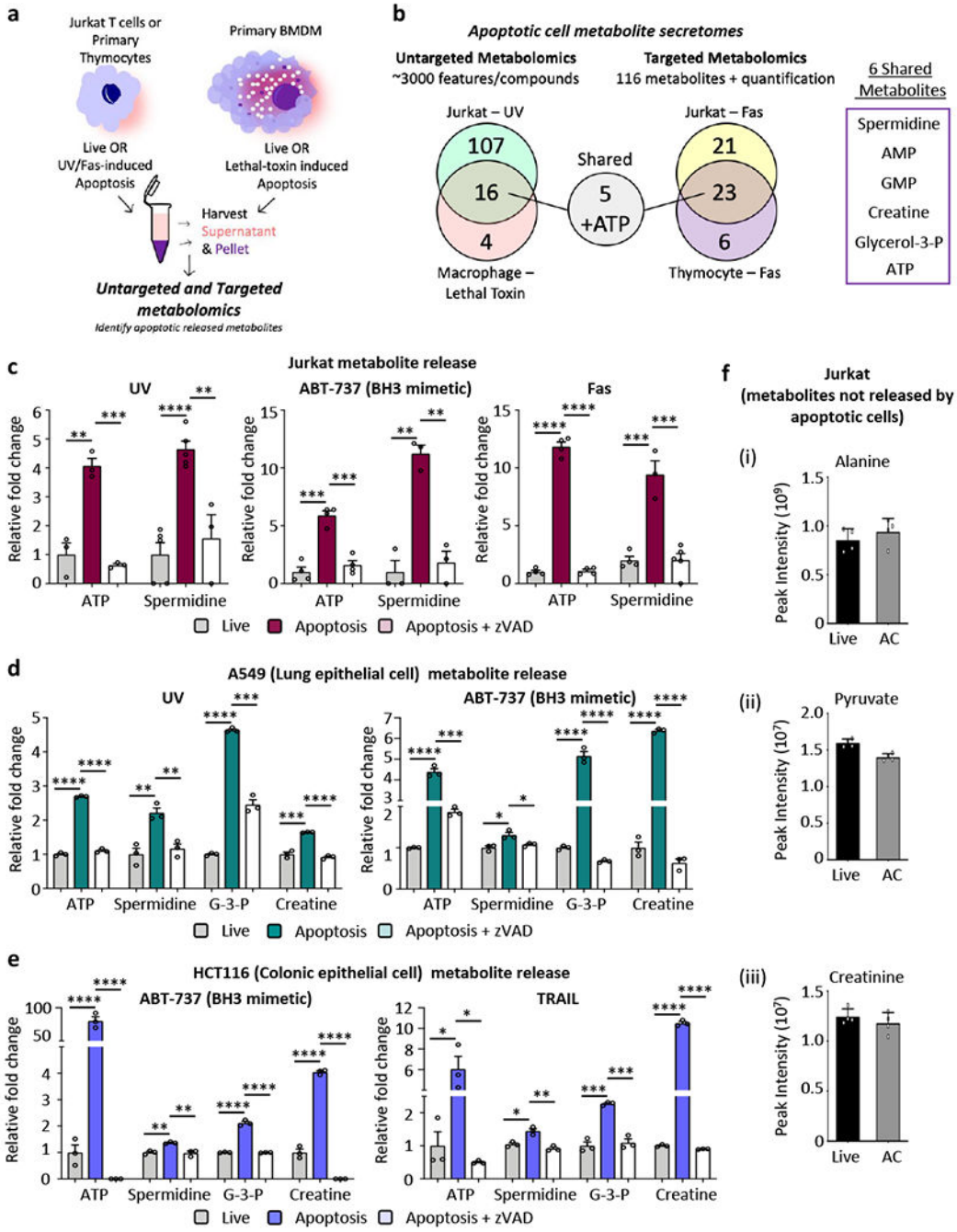

Figure 1. Conserved metabolite secretome from apoptotic cells.

a, Schematic for assessing apoptotic metabolite secretomes**. b,** Venn diagrams illustrating the ‘shared’ apoptotic metabolites identified across cell types, modalities of apoptosis induction, and the two metabolomic platforms tested, and the list of five shared metabolites plus ATP. **c, d, e,** Metabolite release from Jurkat T cells (n=3 for ATP-UV, Spermidine-UV +zVAD, Spermidine-ABT, and Spermidine-Fas. n=4 for ATP-ABT, ATP-Fas, and Spermidine-Fas-live. n=5 for Spermidine-UV-live and Spermidine-Fas+zVAD), A549 lung epithelial cells (n=3), and HCT-116 colonic epithelial cells (n=3) across different apoptotic

stimulus with or without caspase inhibition with zVAD. **f,** Several abundant metabolites such as (i) alanine, (ii) pyruvate, and (iii) creatinine were not released in the Jurkat T cell supernatants (n=4) (* $p < .05$, ** $p < .01$, *** $p < .001$, **** $p < .0001$). Data are mean ± s.e.m (c-e), Data are mean ± s.d (e). Unpaired Student's t-test with Holm-Sidak method for multiple t-tests.

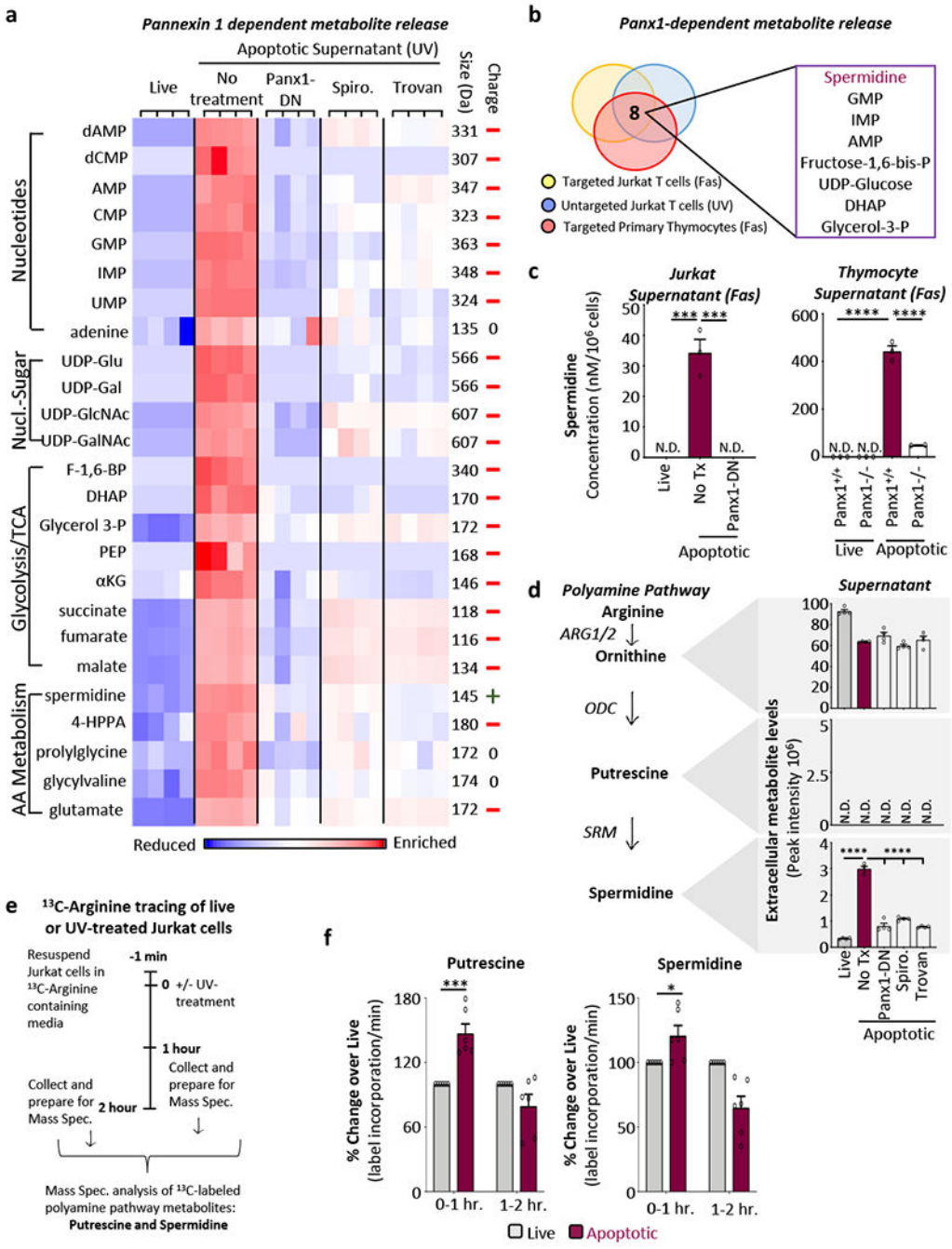

Figure 2. Panx1 activation and continued metabolic activity of dying cells orchestrates metabolite release.

a, Panx1-dependent metabolite release. Heatmap produced from untargeted metabolomics of Jurkat T cell supernatants representing the metabolites that were statistically enriched in the apoptotic supernatants relative to live supernatant ($p < .05$), and reduced when Panx1 was inhibited via a Panx1-DN (genetic), and two Panx1 inhibitors (Spiro and Trovan) (pharmacologic) ($p < .05$). Metabolites are grouped by pathway. Charge and relative sizes (Da) of the metabolites are also shown (n=4). Two-sided Welch's two-sample t-test. **b,**

Three-way Venn diagram (left) illustrating the eight Panx1-dependent apoptotic metabolites observed among the cell types and apoptotic modalities tested. ATP (not detected here) represents the 9th metabolite. **c,** Supernatant spermidine concentration per million cells (targeted metabolomics) from Jurkats (Fas crosslinking - 4 hours - left) (n=3) (***p=0.0002) or primary thymocytes with *Panx1* deletion (Fas – 1.5 hours - right) (n=3) (****p=0.0001). **d,** (left) Schematic of the polyamine metabolic pathway. (right) Relative amounts of ornithine, putrescine, and spermidine in Jurkat T cell supernatants in live and apoptotic conditions, with or without Panx1 inhibition (n=4) (****p=0.0001) **e-f,** Active polyamine metabolic activity during apoptosis. Experimental layout for ^{13}C-arginine labeling (f), and incorporation of ^{13}C-labeled arginine into the polyamine pathway intermediates putrescine (f-left) (***p=0.0003) and spermidine (f-right) (*p=0.025) after cell death induction (n=6). Data are mean ± s.e.m. Ordinary One-way ANOVA, Turkey's multiple comparison test (c,d). Unpaired Student's t-test with Holm-Sidak method for multiple t-tests (e,f).

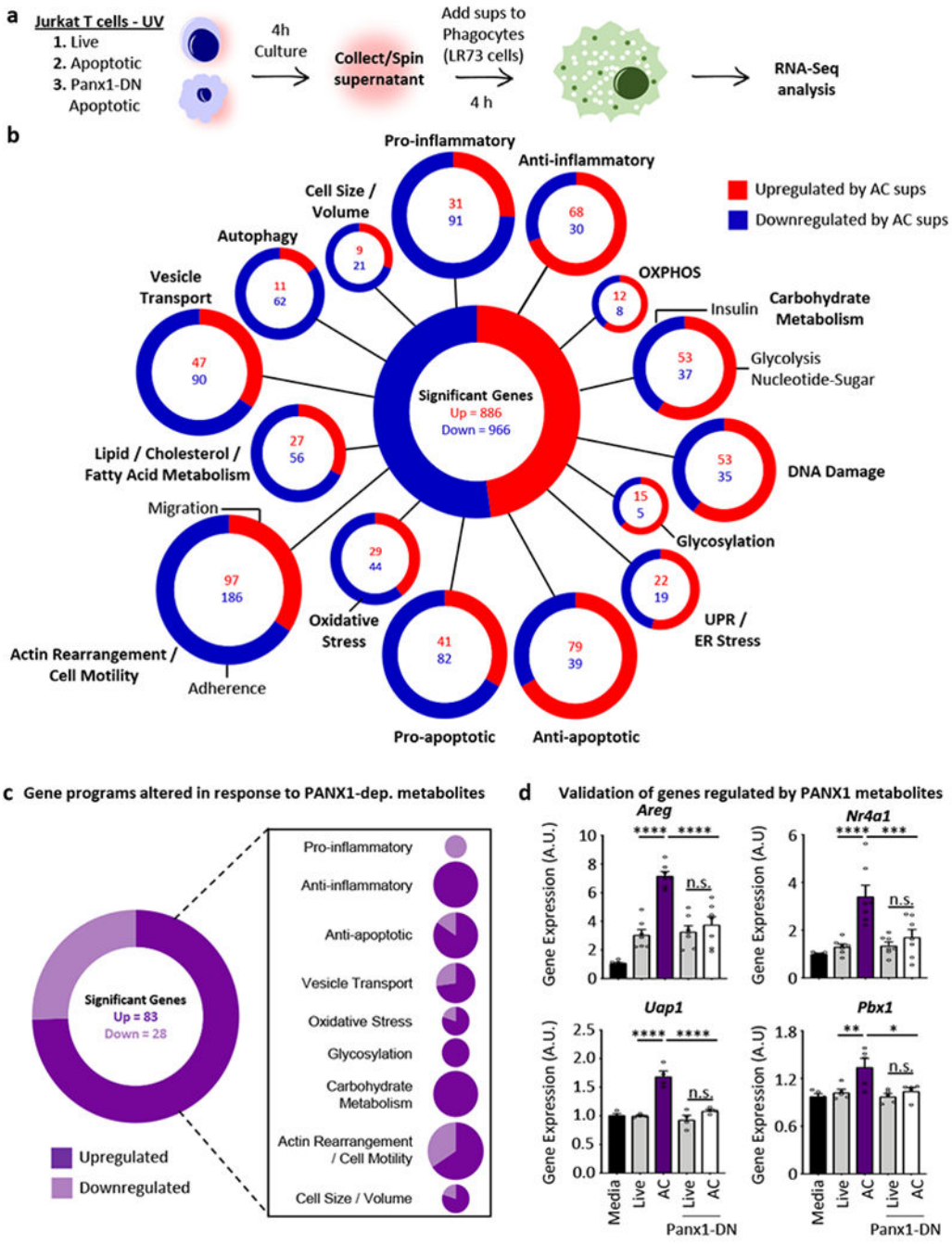

Figure 3. Metabolites from apoptotic cells influence gene programs in live cells.

a, Schematic for assessing gene induction by apoptotic cell supernatants in LR73 cells. **b,** Gene expression programs induced in phagocytes by the apoptotic secretome. Display shows the differentially regulated genes (1852 total, 886 upregulated, 966 downregulated), categorized per known or predicted function(s), literature, and sequence similarity. Circle size is proportional to the number of differentially expressed genes (n=4) (Significance <0.05). **c,** Differentially regulated genes in phagocytes in response to apoptotic cell supernatants with or without pannexin channel inhibition (82 upregulated, 28

downregulated) (n=4). **d,** Validation of genes regulated by Panx1-dependent metabolites. LR73 cells were incubated with indicated supernatants for 4hr, gene expression of *Areg* (n=7) (****p=0.0001), *Nr4a1*(n=7) (Live-AC ****p=0.0001, AC-AC Panx1-DN ***p=0.0008), *Uap1*(n=4) (****p=0.0001), and *Pbx1* (n=5) (Live-AC **p=0.009, AC-AC Panx1-DN *p=0.014) expression in phagocytes. Data are mean ± s.e.m. Ordinary One-way ANOVA, Turkey's multiple comparison test.

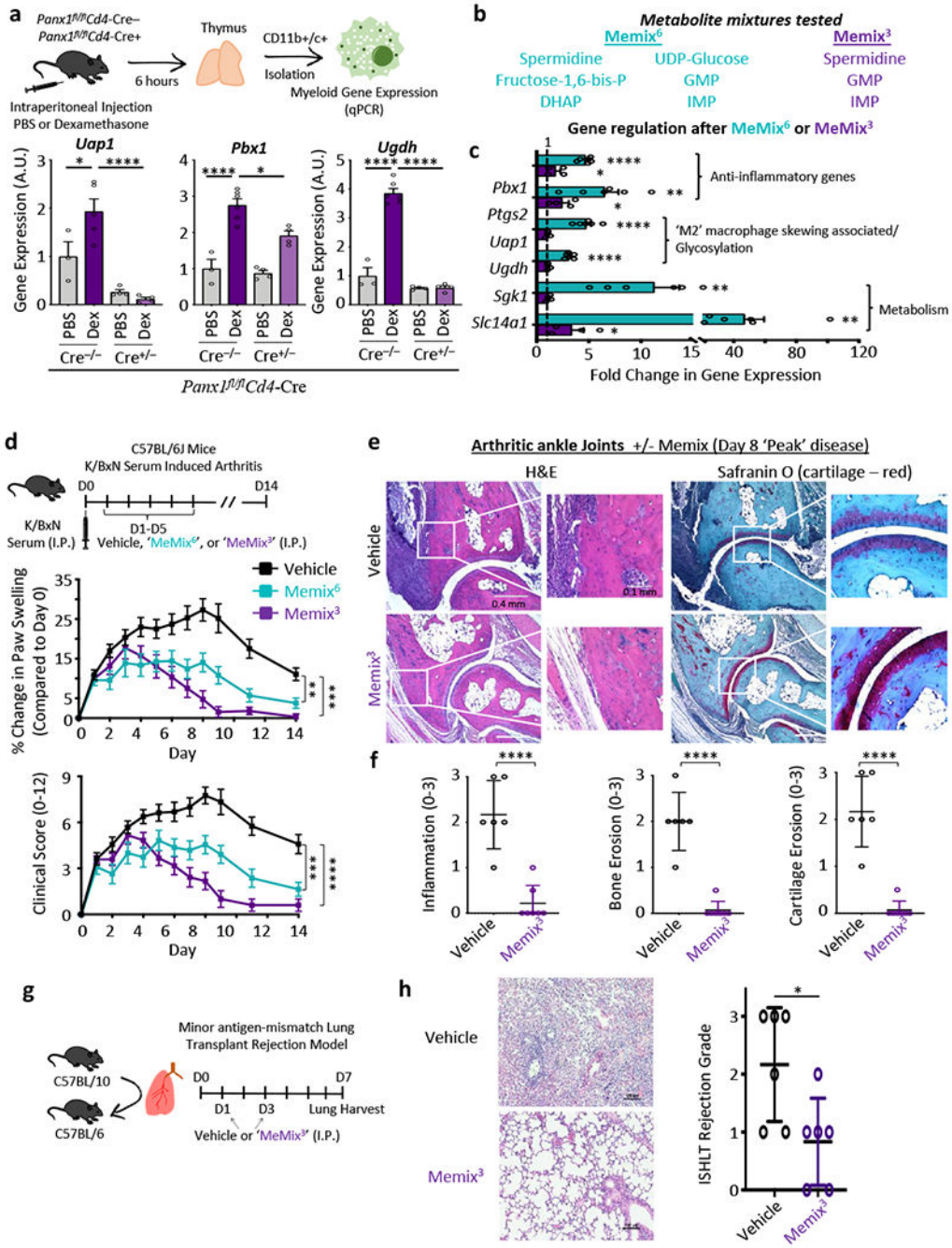

Figure 4. Panx1-dependent metabolite release during apoptosis modulates phagocyte gene expression in vivo and can alleviate inflammation.

a, Panx1 expression in apoptotic thymocytes influences gene expression in myeloid cells *in vivo.* Control mice (Panx1$^{fl/fl}$*, no Cre)* or mice lacking Panx1 in thymocytes (Panx1$^{fl/fl}$ *Cd4*-Cre) were injected with dexamethasone to induce apoptosis in thymocytes (Panx1$^{fl/fl}$ *Cd4*-Cre- PBS n=3, Panx1$^{fl/fl}$ *Cd4*-Cre- Dex n=6, Panx1$^{fl/fl}$ *Cd4*-Cre+ PBS n=4, Panx1$^{fl/fl}$ *Cd4*-Cre+ Dex n=4). After 6hr, CD11b^{+} CD11c^{+} phagocytes were purified for mRNA. qPCR analysis of *Uap1* (WT PBS-WT Dex *p=0.032, WT Dex-KO Dex ****p<0.0001), *Pbx1*

(WT PBS-WT Dex ****p=0.0001, WT Dex-KO Dex *p=0.0103), and *Ugdh* (****p<0.0001) in CD11b+CD11c+ phagocytes. **b,** Panx1-dependent metabolites released from apoptotic cells were compared across cell types and apoptotic conditions to design different metabolite mixtures, *MeMix*^{6} (blue) and *MeMix*^{3} (purple). **c,** *MeMix*^{6} (n=6) and *MeMix*^{3} (n=4) solutions mimic gene expression changes in phagocytes induced by apoptotic supernatants (*p<0.05, **p<0.01, ****p<0.0001). **d,** Schematic of arthritis induction and treatments (top). Paw swelling was measured using a caliper and reported as % change compared to day 0 (*MeMix*^{6} **p=0.0028, *MeMix*^{3} ***p=0.0003). Scores were assessed on a scale of 1-4 per paw (*MeMix*^{6} ***p=0.0004, *MeMix*^{3} ****p=0.0001) (Vehicle n=16, *MeMix*^{6} n=11, *MeMix*^{3} n=12). **e,** Ankle inflammation and bone erosion were scored via H&E staining (left) and Safranin O (right), respectively, from arthritic mouse paws. Increased magnifications of affected areas are also shown. **f,** Clinical analysis of inflammation, bone erosion, and cartilage erosion was scored by an investigator blinded to treatments (Vehicle n=6, *MeMix*^{3} n=7) (****p<0.0001). **g,** *MeMix*^{3} metabolite solution alleviates inflammation in a minor antigen-mismatch lung transplant model. Orthotopic left lung transplantation from C57BL/10 mice into C57BL/6 recipient mice, with *Memix*^{3} administered on post-operation day 1 and 3. Lungs were harvested for histological scoring on day 7. **h,** H&E staining (left) and ISHLT Rejection score (right) (Vehicle n=6, *MeMix*^{3} n=6) (*p=0.024). Data are mean ± s.e.m. (a,c,d). Data are mean ± s.d. (f,h). Ordinary One-way ANOVA, Turkey's multiple comparison test (a). Unpaired two-tailed Student's t-test (c,f,h). Two-Way ANOVA (d).